https://doi.org/10.5194/egusphere-2023-577
Preprint. Discussion started: 7 July 2023

Measurement report: Hygroscopicity of Size-Selective Aerosol Particles at Heavily Polluted Urban Atmosphere of Delhi: Impacts of Chloride Aerosol

Anil Kumar Mandariya[1,2], Ajit Ahlawat[3], Mohd. M. V. Haneef[1], Nisar A. Baig[1], Kanan Patel[4], Joshua S. Apte[5], Lea Hildebrandt Ruiz[4], Alfred Wiedensohler[3]*, and Gazala Habib[1]*

[1]Department of Civil Engineering, Indian Institute of Technology Delhi, New Delhi, India
[2]now at: Univ Paris Est Creteil and University Paris Cité, CNRS, LISA, F – 94010 Créteil, France
[3]Leibniz Institute for Tropospheric Research (TROPOS), Permoserstraße, 15 Leipzig, Germany
[4]Department of Civil, Architectural and Environmental Engineering, The University of Texas at Austin, Austin, Texas, USA
[5]McKetta Department of Chemical Engineering, The University of Texas at Austin, Austin, Texas, USA

Correspondence to: Gazala Habib (gazalahabib@civil.iitd.ac.in) and Alfred Wiedensohler (ali@tropos.de)

Abstract. Recent studies reveal that wintertime chloride emission in the Delhi region is crucial in governing enhancement to theoretically calculated aerosol hygroscopicity and aerosol-bound liquid water to trigger Delhi's fog episodes. Here, we reported that the high volume fractional contribution of ammonium chloride into aerosol governs the high aerosol hygroscopicity and associated liquid water content based on the experimental data first time in Delh. The episodically high chlorides bonded with excess ammonia present in Delhi's atmosphere, which could lead to haze and fog formation under high relative humidity in the region. Therefore, our study suggests that controlling the plastic-contained waste, open burning, and e-waste industrial chloride emission could significantly minimize Delhi's heavily polluted haze/fog events. The high chloride (H-Cl) period was observed significantly ($p<0.05$) higher hygroscopicity (0.35 ± 0.06) compared to high biomass burning (H-BB) (0.18 ± 0.04), high hydrocarbon-like organic aerosol (H-HOA) (0.17 ± 0.05), and relatively cleaner period (0.27 ± 0.07).

In this study, we present the measurement results of bulk aerosol composition of non-refractory PM1 from ACSM and size-resolved (Nucleation, Aitken, and Accumulated mode particles) hygroscopic growth factor and associated hygroscopicity parameter at 90% relative humidity (RH) measured using H-TDMA at Delhi Aerosol Supersite (DAS) first time. The hygroscopic parameter ($\kappa_{H\text{-}TDMA\_90\%}$) was significantly ($p<0.05$) enhanced with the size of the particles. The observed $\kappa_{H\text{-}TDMA\_90\%}$ ranged from .00 to 0.11 (0.03 ± 0.02), 0.05 to 0.22 (0.11 ± 0.03), 0.05 to 0.30 (0.14 ± 0.04), 0.05 to 0.41 (0.18 ± 0.06), and 0.05 to 0.56 (0.22 ± 0.07) for 20, 50, 100, 150, and 200 nm aerosol particles, respectively. The Inorganic-to-organic aerosol ratio in aerosol modulated mainly the aerosol hygroscopicity. In addition, the accumulation mode particle's hygroscopicity was regulated potentially

https://doi.org/10.5194/egusphere-2023-577
Preprint. Discussion started: 7 July 2023

by the volume fraction of NH_4Cl and OA in aerosol particles. Interestingly, our results reveal that the daytime flattening pattern of accumulation aerosol particles in diurnal variation is potentially due to counter the effect of increment of $(NH_4)_2SO_4$ and NH_4NO_3 and decrement of NH_4Cl and OA in aerosol particles.

1. Introduction

The Intergovernmental Panel on Climate Change (IPCC) reported that aerosol-cloud interaction is still not fully understood and has significant uncertainties in quantifying global radiative budgets. Aerosol hygroscopicity plays a pivotal role in overcoming and explaining these uncertainties. Hygroscopicity is crucial to understand how the aerosol particles act as cloud condensation nuclei (CCN) and forms fog droplets/haze at sub-saturated/nearly saturation and cloud droplets at atmospheric supersaturation levels (McFiggans et al., 2006; Topping and McFiggans, 2012). Its understanding is crucial to predict the aerosol size distribution and scattering properties better in global models under varying atmospheric humidity (RH) conditions (Randall et al., 2007). Hygroscopicity at higher RH atmospheric conditions leads to an enhanced aerosol cross-sectional area, resulting in efficient light scattering by the aerosol particles (Tang and Munkelwitz, 1994). It mainly depend on particle size and chemical composition. Generally, the inorganic salts such as ammonium salts of sulfate, nitrate, and chloride, are highly hygroscopic (Hu et al., 2011; Petters and Kreidenweis, 2007), organic aerosol (OA) are comparatively less hygroscopic (Jimenez et al., 2009; Kroll et al., 2011), while dust particles and black/elemental carbon particles are stated as hydrophobic (Seinfeld and Pandis, 2006). Further, the elevated atmospheric RH during winter and monsoon favour the formation of more oxidized secondary organic aerosol (SOA) via aqueous-phase (Ervens et al., 2011) and heterogeneous reactions (McNeill, 2015), leads to enhancement in organic aerosol hygroscopicity (Jimenez et al., 2009; Mei et al., 2013) which adversely impact on the local visibility (Li et al., 2016; Liu et al., 2012). However, aerosol loading inversely affects aerosol hygroscopicity (Mandariya et al., 2020a). Apart from it, aerosol loading is also a critical factor in deciding the lifetime of cloud, which affects the region's rain quantitatively (Albrecht, 1989; Lohmann and Feichter, 2005).

Over the past decades, aerosol hygroscopicity has been intensively measured using hygroscopic tandem differential mobility analyzer (H-TDMA) (Massling et al., 2005; Gysel et al., 2007; Mandariya et al., 2020; Swietlicki et al., 2008; Yeung et al., 2014; Kecorius et al., 2019) and CCN (Bhattu and Tripathi, 2015; Gunthe et al., 2011; Massoli et al., 2010; Ogawa et al., 2016) counter under sub- and supersaturation levels, respectively. Petters and Kreidenweis (2007) introduced a hygroscopicity parameter, kappa (κ), to associate aerosol hygroscopicity with its chemical composition. Furthermore, hygroscopicity associated with OA potentially varies

https://doi.org/10.5194/egusphere-2023-577
Preprint. Discussion started: 7 July 2023

with OA chemical properties like solubility, the extent of dissociation in aerosol water, and surface activity (Hallquist et al., 2009; Jimenez et al., 2009), leads to difficulty in the quantification of OA hygroscopicity, result in introducing more discrepancies in predicted and measured aerosol hygroscopicity. Hence, there is a need to explore measurement-based aerosol hygroscopicity for Delhi's atmosphere to understand the frequent haze/cloud formations better.

In past decades, fast economic growth and industrialization in the IGP led to severe air quality during wintertime (Wester et al., 2019). Delhi is potentially affected by local and regional air pollution problems in wintertime (Arub et al., 2020; Bhandari et al., 2020; Gani et al., 2019; Prakash et al., 2018). Recent studies (Gani et al., 2019; Rai et al., 2020) have shown chloride is one of the predominant factors to degrade the air quality in the Delhi region and significantly favour the haze/fog formation during winter (Gunthe et al., 2021). Trash and biomass burning for heating and waste degradation are among the main contributors to chloride in Delhi (Rai et al., 2020). A recent study conducted in Delhi reported that frequent high chloride events promotes high aerosol liquid water content under elevated humid condition leads to haze and poor visibility in the city (Chen et al., 2022). In addition, Gunthe et al. (2021) showed higher chloride also facilitates enhancement in aerosol hygroscopicity, however, this study was based on theoretical hygrocopicity. Therefore, it is essential to investigate the impacts of chloride on aerosol hygroscopicity and its potential to enhance aerosol-bound liquid water based on field measurements. Moreover, the hygroscopicity of the aerosol particles in the heavily polluted urban atmosphere, which confines to highly complex composition, is very limited, like Delhi, situated at Indo Gangetic Plain (IGP), India, where air quality severely degrades during haze/fog-dominated. To the author's best knowledge, the current study is first in Delhi, India, exploring a complex atmosphere of IGP using H-TDMA-measured aerosol hygroscopicity. Hence, it is essential to measure size-resolved aerosol hygroscopicity in Delhi's atmosphere and investigate its role in the context of high chloride.

2. Experimental Methods

2.1 Aerosol Measurements

Real-time atmospheric aerosol measurements were conducted simultaneously using Hygroscopic-Tandem Differential Mobility Analyzer (H-TDMA) and Aerodyne Aerosol Chemical Speciation Monitor (ACSM, Aerodyne Research, Billerica MA) during winter (1st February 2020 to 16th March 2020) at the Indian Institute of Technology (IIT) Delhi in Block 5, at the height of nearly 15 m. Details on the sampling site can be found in Arub et al. (2020). In this study, the HTDMA system was used to investigate the hygroscopic growth of size-resolved

https://doi.org/10.5194/egusphere-2023-577
Preprint. Discussion started: 7 July 2023

particles at 90 % RH. The HTDMA system has been previously used in many field campaigns (Massling et al., 2007; Wu et al., 2013b; Zhang et al., 2016). The HTDMA system (TROPOS, Germany) is comprised of two Differential Mobility Analyzers (DMAs, type Hauke-median, TROPOS, Germany), a Condensation Particle Counter (CPC, Model 3772, TSI Inc., USA) along with a humidifier system located between the two DMAs. The role of first DMA is to select the quasi-monodisperse particles at a dry diameter (*D*p, dry) with 30% RH. After that, the size-selected particles pass through a humidity conditioner, which can be adjusted from 30% to 90% RH by regulating the aerosol and sheath air flow by mixing dry air with RH<5% and humid air with ~95% RH (Maßling et al., 2003). The uncertainties associated with RH measurement at 90% RH is 1.0%. The particle hygroscopic growth distribution at dry size (*D*p, dry) at a certain humidity can be easily determined with CPC. There are two humidity sensors (Vaisala) in the system for aerosol and sheath respectively. The humidity sensors positioned in the second DMA were calibrated automatically with 100 nm ammonium sulfate ((NH4)2SO4) particles every 30 min at 90% RH to analyze the stability at high RH. The measurement error of the HTDMA mainly depends on the uncertainty in measuring and controlling the RH within the system (Su et al., 2010). Therefore, all RH sensors were calibrated using the Vaisala salt kit comprising LiCl, NaCl, KCl etc. prior the measurement campaign. Both the DMAs were size calibrated by applying the Latex particles with the standard size of 200 nm before the start of the measurement. The number concentration peak occurred at 203 nm, referring to accuracy of DMAs size selection at 1.5%. HTDMA system was operated at 90% RH to measure the hygroscopic growth factors (HGFs) for particles with *D*p, dry of five different sizes i.e. 20, 50, 100, 150 and 200 nm. The time resolution of the full scan covering the five sizes was about 30 min.

ACSM was operated at nearly 0.1 lpm at 1 min time resolution in a temperature-controlled laboratory. ACSM was set to run to measure mass-to-charge ratio (m/z) m/z 10 to m/z 140. The ACSM measures non-refractory particulate matter less than 1µm (NR-PM_1). The concentrate PM_1 aerosol beam was impacted on the vaporizer at 600 °C and flash-vaporized compounds were subsequently ionized through impact ionization at 70 eV electron and detected with a quadrupole mass spectrometer (Ng et al., 2011). The 200 ms amu^{-1} scan speed and pause setting at 125 for a sampling time (64 s) were set to acquire aerosol mass spectra in ACSM. Detailed operational procedures for the ACSM are explained elsewhere in Gani et al. (2019).

2.2 Data Analysis

2.2.1 ACSM

https://doi.org/10.5194/egusphere-2023-577
Preprint. Discussion started: 7 July 2023

Details on ACSM calibration and data processing are in Patel et al., 2021. We conducted Positive matrix factorization (PMF) on the data and found a four-factor solution (hydrocarbon-like OA, "HOA"; biomass burning OA, "BBOA"; less-oxidized OA, "LO-OOA"; more-oxidized OA "MO-OOA) to best represent the data set. Further details about PMF analysis are in section S.1 of the SI.

The windrose plot was plotted by openair in R package (http://www.r-project.org, http://www.openair-project.org). The 48-hour back trajectory of air masses reaching Delhi super site (DSL) at 500 m above the ground at every hour for the entire study period was estimated by an offline based Hybrid Single-Particle Lagrangian Integrated Trajectory (HYSPLIT4) model developed by NOAA/Air Resources Laboratory (ARL)) (Draxler and Hess, 1997). The input meteorological data for back trajectories were taken from the Global Data Assimilation System (GDAS 0.5 degree) archive maintained by ARL (http://ready.arl. noaa.gov/archives.php). Further, utilizing these estimated back trajectories as input combined with the measured mass fraction of chemical species of bulk aerosol, Potential Source Contribution Function (PSCF) analysis was carried out with the help of a tool called Zefir (V 3.7) written in Igor Pro (WaveMetrics). Detail description regarding Zefir tool can be found elsewhere (Petit et al., 2017). In addition, box plots reported in the subsequent section were also plotted with the help of this tool. The aerosol liquid water content (ALWC) as a function of inorganic species mass concentration, ambient temperature (T), and ambient relative humidity (RH), was calculated by ISORROPIA-II model (Fountoukis and Nenes, 2007).

2.2.2 H-TDMA

The humidity sensor of DMA2 was automatically calibrated with 100 nm ammonium sulfate particles after each scan cycle. Overall, we recorded 1483 H-TDMA scans cycles. Afterward, the % difference between measured and theoretical growth factors (say Δq) was calculated after each scan cycle for 100 nm ammonium sulfate particles. Those scan cycles came between $\Delta q \leq \pm 5\%$, were only carried out for further data treatment, and the rest scans cycles were discarded (Kecorius et al., 2019). Thus, we had 1102 H-TDMA scan cycles following this data quality check. Regarding good scan cycles, we had 1449, 1431, 1438, 1470, and 1420 good H-TDMA scans for 20, 50, 100, 150, and 200 nm particles, respectively, to further analyze. Afterward that, a piecewise linear TDMAinv algorithm, namely TDMAinv Toolkit, written in IgorPro and developed by Gysel et al. (2009), was used to do post-data treatment on the raw HGF. Because the measured distribution function is a skewed and smoothed integral transform of the actual growth factor probability density functions (GF-PDFs). A detailed description of the raw data processing in the TDMAinv toolkit to measure real HGFs is described in Gysel et al.

https://doi.org/10.5194/egusphere-2023-577
Preprint. Discussion started: 7 July 2023

(2009). The TDMAinv toolkit was successfully used in various studies around the globe (Gysel et al., 2007; Liu et al., 2012; Sjogren et al., 2007; Wang et al., 2018a) and at Kanpur, India (Mandariya et al., 2020a). Besides, the RH in the DMA2 generally achieved the set value of 90% and remained stable within ±1%, although occasionally, it faced a more considerable drift. All growth factors measured between 88 and 92% RH were corrected to a target value of 90% (HGF_90%) (Gysel et al., 2007) using the kappa-model suggested in the TDMAinv toolkit (Gysel et al., 2009) to minimize this DMA2 RH drifts. After it, 979, 957, 972, 969, and 966 scans were found corrected at target RH for 20, 50, 100, 150, and 200 nm aerosol particles, respectively, which further averaged for 60 min time resolution and finally, these numbers reached to 425, 429, 419, 424, and 417, respectively.

Further, size-resolved hygroscopicity factors (kappa, κ, say $\kappa_{\text{H-TDMA\_90\%}}$) were calculated from the respective size-resolved target RH corrected HGFs using equation (1) kappa-Köhler theory (Mandariya et al., 2020a; Petters and Kreidenweis, 2007).

$$\kappa_{H-TDMA\_90\%} = (HGF\_90\%^3 - 1)\left[\frac{1}{RH}\, exp\; exp\; \left(\frac{4\sigma M_w}{RT\rho_w D_O HGF\_90\%}\right) - 1\right] \quad (1)$$

Where, $\kappa_{\text{H-TDMA\_90\%}}$ is the hygroscopicity factor at 90% RH, HGF_90% is the size-resolve HGF at 90% RH, RH is the atmospheric relative humidity in fraction, σ is the surface tension of the aerosol liquid droplet-air interface at the droplet surface in N/m and can be assumed nearly to pure water, R is the universal gas constant in J K^{-1} mol^{-1}, M_w is the molecular mass of water, T is the ambient temperature in Kelvin (K), ρ_w is the density of water in kg/m^3, and D_o is the dry mobility diameter of the particle in m.

2.2.4 Derived Secondary Inorganic Salts

The ACSM mainly measures OA, NO_3, SO_4, NH_4, and Cl. Therefore, we adopted a simplified ion-pairing scheme reported by Gysel et al. (2007). However, Gysel et al. (2007) did not include NH_4Cl in their ion-pairing scheme; therefore, we elaborated this scheme and made some modifications in this scheme to include ACl in the calculation. Hence, our modified ion-pairing scheme includes ACl, AN, AS, ABS, and SA are shown below:

Case-1 $\boldsymbol{R_{SO_4}(NH_4\ to\ SO_4) \leq 1}$

$$SA = 98.0795 \times \max(0, (n_S - n_A))$$

$$ABS = 115.11 \times n_A$$

$$AS = 0$$

https://doi.org/10.5194/egusphere-2023-577
Preprint. Discussion started: 7 July 2023

174 $$AN = \left(\min\left(\left(n_A - \left(\frac{ABS}{115.11} \right) - \left(\frac{(2 \times AS)}{132.1405} \right) \right), n_N \right) \right) \times 80.0434$$

175 $$ACl = \left(\min\left(n_C, \left(n_A - \left(\frac{ABS}{115.11} \right) - \left(\frac{2 \times AS}{132.1405} \right) - \left(\frac{AN}{80.0434} \right) \right) \right) \right) \times 53.54$$

176 **Case-2 $1 < R_{SO_4} < 2$**

177 $SA = 0$

178 $ABS = 115.11 \times ((2 \times n_S) - n_A)$

179 $AS = 132.1405 \times (n_S - n_A)$

180 $$AN = \left(\min\left(\left(n_A - \left(\frac{ABS}{115.11} \right) - \left(\frac{(2 \times AS)}{132.1405} \right) \right), n_N \right) \right) \times 80.0434$$

181 $$ACl = \left(\min\left(n_C, \left(n_A - \left(\frac{ABS}{115.11} \right) - \left(\frac{2 \times AS}{132.1405} \right) - \left(\frac{AN}{80.0434} \right) \right) \right) \right) \times 53.54$$

182 **Case-3 $R_{SO_4} \geq 2$**

183 $SA = 0$

184 $ABS = 0$

185 $AS = 132.1405 \times n_S$

186 $$AN = \left(\min\left(\left(n_A - \left(\frac{ABS}{115.11} \right) - \left(\frac{(2 \times AS)}{132.1405} \right) \right), n_N \right) \right) \times 80.0434$$

187 $$ACl = \left(\min\left(n_C, \left(n_A - \left(\frac{ABS}{115.11} \right) - \left(\frac{2 \times AS}{132.1405} \right) - \left(\frac{AN}{80.0434} \right) \right) \right) \right) \times 53.54$$

https://doi.org/10.5194/egusphere-2023-577
Preprint. Discussion started: 7 July 2023

Here, n denotes the number of moles, whereas A, N, S, and C denotes the NH_4, NO_3, SO_4, and Cl species. We also predicted these inorganic salts concentrations from the ISORROPIA v2.1 model using NH_4, SO_4, NO_3, and Cl. We found a strong correlation and nearly unit slope (0.9999) between the calculated and modelled inorganic salts as presented in figure S1, which strongly justifies the new ion-pairing scheme adopted in this study.

3. Result and Discussions

3.1 Overview of meteorology, trace gases, and aerosol characterization

Meteorological parameters provided a quick summary of the local weather conditions at the sampling site. Figure 1 shows the hourly resolved temporal variability of meteorological parameters (RH, T, WD, and WS), particle number size distribution (PNSD), particle volume size distribution (PVSD), principal components in non-refractory PM_1 and OA and their fractional mass contribution. In addition, the temporal variability in the atmospheric gases (NOx, CO, and SO_2) have shown in figure S5. Delhi's winter climate is mainly influenced by a depression created by the Western Disturbances caused by cold waves in the region. The ambient relative humidity (RH) and temperature (T) variability between 24.2–96.6% and 9.0–28.5°C with an average (±1 STD) of 56.0 ± 18.2% and 18.7 ± 4.2°C, respectively, showed the Delhi's atmosphere was varied from wet and cold to dry and relatively warm from February to March, respectively. The nighttime was somewhat cold and humid compared to the daytime throughout the sampling. The ambient RH showed a diurnal pattern with a peak during early morning 06:00-07:00 hr and the valley during noontime 13:00-15:00 hr, while ambient temperature showed an opposite trend with a rise during noontime could be correlated with noontime higher solar radiation. This comparatively higher ambient temperature and O_3 peak concentration during noontime indicate the daytime photooxidation process.

The wind speed (WS) and wind direction (WD) varied from 0.0 to 5.6 (1.0 ± 1.0) m/s and 4.0 to 345.7 (197.1 ± 84.4) degrees from the North, respectively, as shown in figure S6. Predominant wind directions were WNW-WSW and E-ESE. It indicates that the atmosphere remained stagnant during the study period, and measured aerosol potentially represents Delhi's emissions and local aerosol chemistry.

Furthermore, ambient trace gases NOx and CO showed substantial variability during the sampling period, with a peak in local burning activities. During intensely biomass burning activities, ambient NOx ambient level reached a maximum of 421.2 ppb (58.4 ± 61.9). Moreover, the CO showed peak level at similar periods as NOx, and its concentration varied from 0.0 to 7.66 ppm (0.58 ± 0.79), as shown in figure S5. The diurnal variation of trace gases is shown in figure 2 (f, g, h, and i). The CO and NOx concentrations showed two peaks in days (06:00-

https://doi.org/10.5194/egusphere-2023-577
Preprint. Discussion started: 7 July 2023

08:00 and 17:00-20:00), attributed to the morning local biomass/trash burning emissions, night-time traffic rush hours, and regional biomass burning activities. Besides, SO_2 showed a different trend from CO and NOx. SO_2 varied dynamically from 0.46 to 9.55 ppb (4.41 ± 1.20) and showed a peak during the morning (09:00-12:00 hr) and midnight (21:00 to 02:00 hr).

PM_1 particle number concentration varied from 408 to 29845 /cm^3 (11319 ± 5552). High particle number concentrations generally observed were associated with local burning events. The particle concentration increased in the evening (at 18:00 hr) and reached its maximum value at midnight, as shown in figure 2(e). This time generally indicates the resumption of residential burning activity and traffic emissions. These activities probably caused the lower geometric mean diameter (GMD) (≈ 47 nm) of the particle number size distribution (PNSD), which further increased nearly up to 87 nm, as shown in figure 2(t), pointing out the night-time aging of organic aerosol. The hourly averaged mean diurnal GMD of PVSD varied from nearly 274 to 324 nm, as indicated in figure 2(y). However, during the sampling period, its variation was observed to vary between 221.3 and 418.4 nm with the mean value of 309.1 ± 33.1 nm, which is close to this study's higher-end particle size of 200 nm hygroscopicity measurement. Therefore, ACSM bulk aerosol composition could be the best choice for discussing the hygroscopicity of 200 nm aerosol particles.

The hourly time-resolved NR-PM_1 (say hereafter PM_1) concentration varied from 9.0 to 357.9 µg/m^3, averaging 81.2 ± 56.6 µg/m^3. This observation lies well within the boundary of 12.7-392 µg/m^3 (NR-PM_1), reported by Gani et al. (2019) for the current site. Prakash et al. (2018) said that PM_1 mass concentration is 83% of $PM_{2.5}$, representing the dominance of combustion-based particles. Further, we observed that ACSM measured NR-PM_1 (PM_1) was highly correlated (r^2 = 0.83, $p<0.05$) with MPSS measured PM_1, assuming an effective aerosol density 1.6 g/cm^3 (figure S2). It means that a substantial mass of PM_1 was composed with non-refractory material and other refractory material like black carbon, metals and crustal material, which was not measured in the current study, constituted less than 5% of PM_1 (Prakash et al., 2018). OA was the predominant fraction of PM_1 with an average mass concentration of 46.5 ± 39.6 µg/m^3, consistent with 112 µg/m^3 observed during winter (December-February) at the present site (Gani et al., 2019). However, lower OA concentration could be explained by the measuring period of February-March, as aerosol loading starts decreasing in February after reaching its peak in December-January (Gupta and Mandariya, 2013). Campaign average fractional contribution OA to PM_1 was 56%, ranging from 1 to 84%. This high OA contribution in PM_1 is consistent with other studies conducted in IGP (Chakraborty et al., 2016a; Gani et al., 2019; Mandariya et al., 2019) and worldwide (Jimenez et al., 2009; Zhang et al., 2007). Peaked OA mass concentrations were noted between 21:00-23:00 hr (figure 2(k)), consistent with

https://doi.org/10.5194/egusphere-2023-577
Preprint. Discussion started: 7 July 2023

247 previous studies conducted at the current site (Gani et al., 2019; Rai et al., 2020). Campaign average mass
248 concentration of NO_3 was 10.1 ± 7.0 µg/m^3 and showed diurnal variation with a peak in the morning and midnight
249 (figure 2(l)). Besides, SO_4 showed slight enhancement at 08:00 hr and remained nearly constant from noon to
250 17:00 hr (figure 2(m)). However, Cl varied between 0.13 to 77.83 µg/m^3, and higher concentrations of Cl were
251 found episodic throughout the campaign. The Cl- concentration was found consistent with Gani et al., 2019's
252 previously reported value of 0.1-66.6 µg/m^3 at the current site. Figure 1 shows the temporal variation of all
253 possible OA factors. BBOA mass concentration varied between 0.0 to 134.7 µg/m^3. The two peaks during the
254 night (21:00-23:00 hr) and morning (07:00-08:00 hr) featured the BBOA diurnal variation (figure 2(r)). Besides,
255 LO-OOA diurnal variation peaked in the morning (10:00 hr) and remained nearly flattered at noontime. It could
256 indicate its steady formation rate. However, the diurnal variation of MO-OOA showed a slight bump during
257 noontime, indicating its formation via daytime photooxidation (Mandariya et al., 2019; Sun et al., 2016). Overall,
258 oxygenated organic aerosol (OOA) was the dominant fraction of OA during the sampling period.

259 Furthermore, based on the variability in aerosol chemical composition, three different events were observed: first,
260 high-residential or local biomass burning (H-BB), second, high-hydrocarbon like OA (H-HOA), and third, high-
261 chloride (H-Cl) period, characterized by high BBOA, HOA, and Cl, respectively. In addition, we also classified
262 a "Clean Period" where PM_1 loading was less than 25 percentile (≤ 38.7 µgm^{-3}) of the sampling period. H-BB
263 events showed a dynamic variation in BBOA mass concentration from 16.3 to 134.7 (50.7 ± 24.0) µg/m^3.
264 Although, a higher mass concentration of HOA (9.6 – 109.4 µg/m^3) was also observed in these events. It indicates
265 that HOA also has probably similar sources during this event. Nevertheless, a higher HOA concentration (4.8-
266 58.9 µg/m^3) was noted during H-HOA events, although these concentrations were significantly lower than those
267 observed during H-BB events. Nevertheless, fractional mass contribution of HOA to OA was largest among all
268 OA species. Besides, H-Cl events observed a higher concentration of both primary organic aerosol HOA and
269 BBOA. BBOA contributed nearly 40.0, 21.1, 32.5, and 13.1% to OA during H-BB, H-HOA, H-Cl, and relatively
270 clean events, respectively, indicating different BBOA sources. Besides, the HOA's average contribution of 41.6%
271 was observed in the H-HOA event was the highest among all events. In addition, Cl's fractional mass contribution
272 in PM_1 reached up to 44.9% in the H-Cl event compared to 21.2% (H-BB) and 7.3% (H-HOA) events.

https://doi.org/10.5194/egusphere-2023-577
Preprint. Discussion started: 7 July 2023

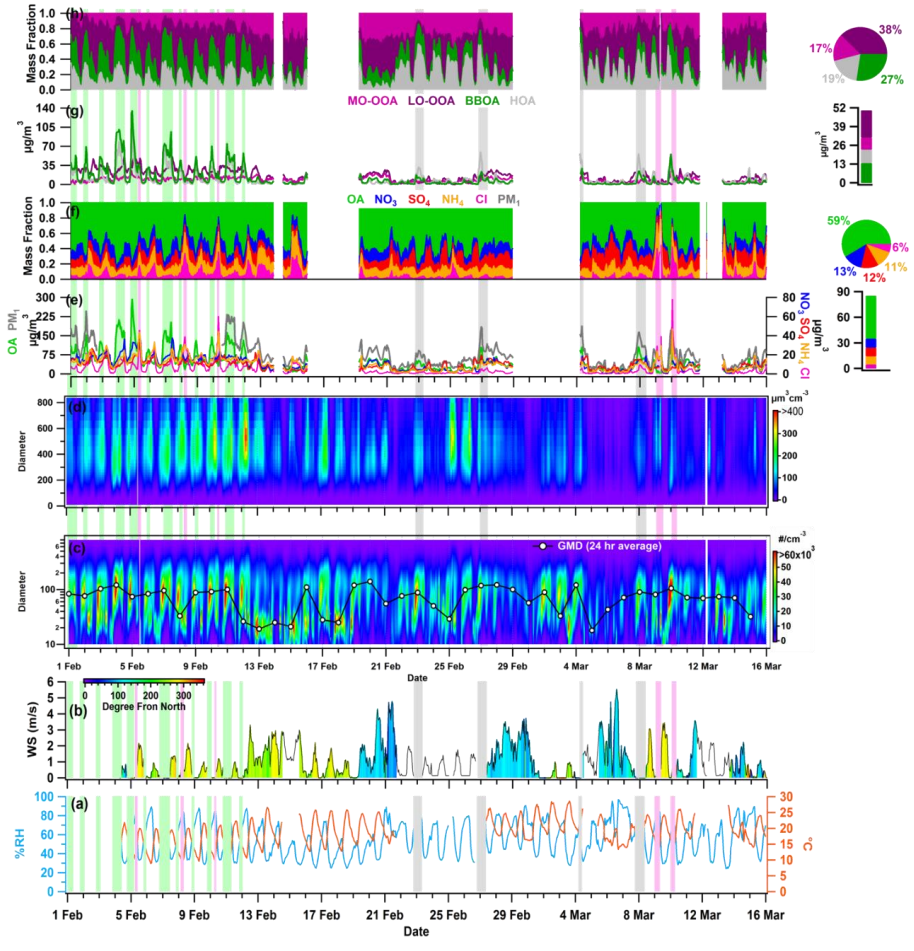

Figure 1: Temporal variability of ambient (a) relative humidity (RH), temperature (T), (b) wind speed (WS), wind direction (WD), (c) particle number-size distribution (PNSD), 24-average geometric mean diameter (GMD), (d) particle volume-size distribution (PVSD), (e) particulate matter (PM_1), organic aerosol (OA), nitrate (NO_3), sulfate (SO_4), ammonium (NH_4), chloride (Cl), (f) fractional contribution of OA, NO_3, SO_4, NH_4, and Cl in PM_1, (g) more oxidized-oxygenated OA (MO-OOA), less oxidized-oxygenated OA (LO-OOA), biomass burning OA (BBOA), hydrocarbon like-OA (HOA), and (h) fractional contribution of MO-OOA, LO-OOA, BBOA, and HOA in OA. The pie chart sub-plot represents the overall average contribution of species, and the bar sub-plot represents the overall campaign average value of different species. All other species are represented with specific color coding mentioned in legends.

https://doi.org/10.5194/egusphere-2023-577
Preprint. Discussion started: 7 July 2023

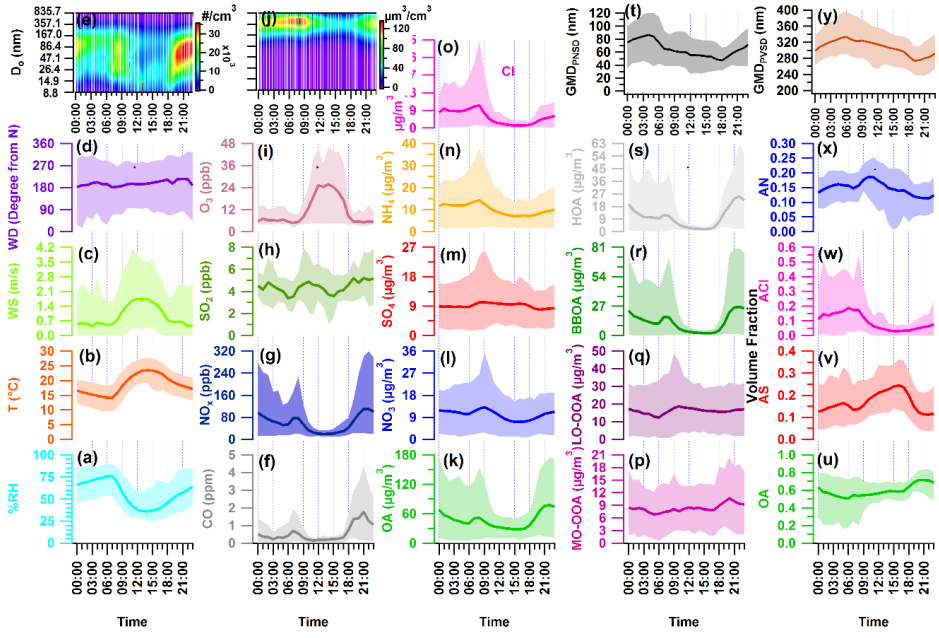

Figure 2: Diurnal variation of ambient meteorological parameters (a) % ambient relative humidity (RH), (b) temperature (T), (c) wind speed (WS), (d) wind direction (WD), and (e) particle number size distribution (PNSD), mass concentration of ambient trace gases (f) carbon mono-oxide (CO), (g) nitrogen oxides (NOx), (h) sulfur dioxide (SO_2), and (i) ozone (O_3), (j) particle volume size distribution (PVSD), mass concentration of aerosol constituents (k) organic aerosol (OA), (l) nitrate (NO_3), (m) sulfate (SO_4), (n) ammonia (NH_4), and (o) chloride (Cl), mass concentration of organic aerosol species (p) more oxidized-oxygenated OA (MO-OOA), (q) less oxidized-oxygenated OA (LO-OOA), (r) biomass burning OA (BBOA), and (s) hydrocarbon like-OA (HOA), (t) geometric mean diameter of particle number size distribution (GMD_{PNSD}) and volume fractional contribution of (u) organic aerosol (OA), (v) ammonium sulfate (AS), (w) ammonium chloride (ACl), and (x) ammonium nitrate (AN) in PM_1, and (y) geometric mean diameter of particle volume size distribution (GMD_{PVSD}). Upper and lower boundary of shaded area represents the 95th and 5th percentile values of respective species.

3.2 Hygroscopicity of Nucleation, Aitken, and Accumulation Mode Particles

3.2.1 Temporal variability

Figure 3 shows the dynamic variability in the hourly averaged $HGF_{90\%}$ and hygroscopicity parameter ($\kappa_{H\text{-}TDMA\_90\%}$, kappa) of Nucleation, Aitken, and Accumulation mode aerosol particles at 90% ambient relative humidity. The hygroscopic growth factors of 20 ($HGF_{90\%\_20nm}$), 50 ($HGF_{90\%\_50nm}$), 100 ($HGF_{90\%\_100nm}$), 150 ($HGF_{90\%\_150nm}$), and

https://doi.org/10.5194/egusphere-2023-577
Preprint. Discussion started: 7 July 2023

200 nm ($HGF_{90\%\_200nm}$) size particles varied between 1.00-1.41, 1.05-1.39, 1.11-1.49, 1.12-1.63, and 1.12-1.179 with an average of 1.14 ± 0.09 (average ± standard deviation), 1.16 ± 0.06, 1.27 ± 0.07, 1.35 ± 0.09, and 1.41 ± 0.09, respectively. These mean hygroscopic growth factors were noted as statistically ($p<0.05$) different from each other. In addition, the hygroscopicity ($\kappa_{20nm\_90\%}$ and $\kappa_{50nm\_90\%}$) of 20 and 50 nm aerosol particles varied between 0.00-0.11 and 0.02-0.25, with an average of 0.03 ± 0.02 and 0.09 ± 0.03, respectively. Nucleation mode particles were observed, mainly monomodal GF-PDF (figure 3(a)), comprising nearly 74±24% nearly hydrophobic particles (HGF <1.2). However, this contribution was raised to 100%, which was observed to have a good association with night-time local burning activities, as shown in the figure 3(a). The nucleation mode particles ($\kappa_{20nm\_90\%}$) showed significantly ($p<0.05$) lower hygroscopicity than Aitken mode particles ($\kappa_{50nm\_90\%}$). Hong et al. (2015) reported that nucleation mode particles are more sensitive to condensable vapors like fresh VOCs, H_2SO_4 and HCl. However, the present study did not measure these species. The κ of Aitken size particles were comparable with 0.24 ± 0.08 of 52.6 ± 6.9 size particles reported by Gunthe et al. (2011) for Beijing. Beijing is also one of the most polluted urban locations like Delhi, which could justify the comparison. However, Gunthe et al. (2011) performed this study using CCN on supersaturation levels. The campaign average hygroscopicity parameter (kappa, $\kappa_{90\%}$) increased significantly ($p<0.05$) with particle size, which can be attributed to the kelvin effect (Wang et al., 2018a). In the accumulation size range (100, 150, and 200 nm), $\kappa_{90\%}$ increased to ~0.56. The overall sampling average values of $\kappa_{100nm\_90\%}$, $\kappa_{150nm\_90\%}$, and $\kappa_{200nm\_90\%}$ were 0.14 ± 0.04, 0.18 ± 0.06, and 0.22 ± 0.07, respectively. The $\kappa_{200nm\_90\%}$ varied between 0.05 and 0.56. The similar kind of variation in κ with particle size has been demonstrated in Kanpur, situated at the center of IGP, India (Mandariya et al., 2020a) and worldwide studies (Cerully et al., 2015; Enroth et al., 2018; Fan et al., 2020; Kawana et al., 2016; Kim et al., 2020; Kitamori et al., 2009; Ogawa et al., 2016; Sjogren et al., 2012; Wang et al., 2018a). Moreover, this was attributed to the predominant increment in inorganic to OA fraction in particles with increment in size. Furthermore, $\kappa_{H\text{-}TDMA\_90\%}$ was found approximately in the 0.13-0.77, reported by Arub et al. (2020) at Delhi for PM_1 without considering BC. Although, Arub et al. (2020) theoretically predicted particles' hygroscopicity by considering a particle's chemical composition. They found a decrease in κ calculation by 10% when BC was considered in aerosol chemical composition. Also, $\kappa_{H\text{-}TDMA\_90\%}$ measured in the current study were found in line with the global average value of 0.27 ± 0.21 for continental aerosols (Petters and Kreidenweis, 2007; Pringle et al., 2010). Further, to understand the impact of a particle's chemical composition, local meteorology, and air mass trajectories on $\kappa_{H\text{-}TDMA\_90\%}$ for accumulation mode particle discussed in subsequent sections.

https://doi.org/10.5194/egusphere-2023-577
Preprint. Discussion started: 7 July 2023

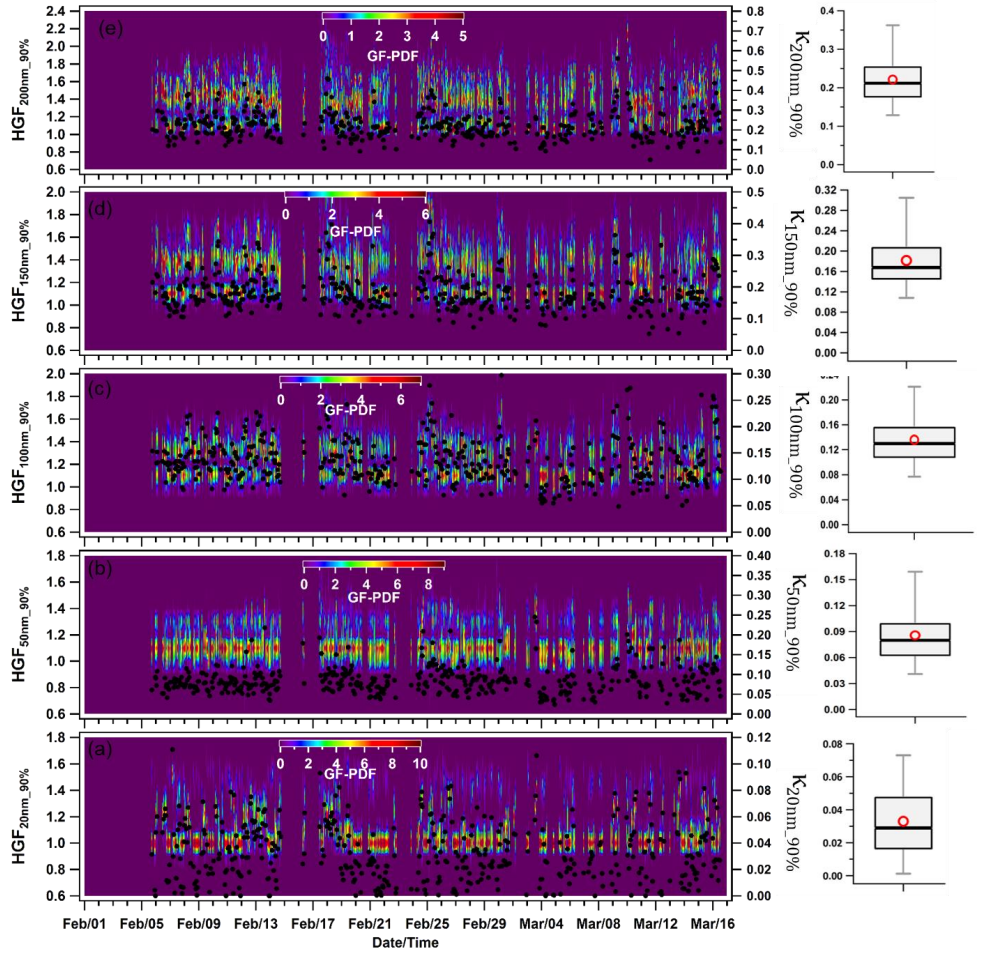

Figure 3: Temporal variability in hygroscopic parameter kappa (κ) of nucleation mode particles (a) 20 nm ($\kappa_{20nm\_90\%}$), Aitken mode particles (b) 50 nm ($\kappa_{50nm\_90\%}$), and Accumulation mode particles (c) 100 nm ($\kappa_{100nm\_90\%}$), (d) ($\kappa_{150nm\_90\%}$), and (e) 200 nm ($\kappa_{200nm\_90\%}$). The box plots represent the variability in the hygroscopicity of respective sizes of particles in which low and high whisker traces represent the 5 and 95 percentile, respectively. The red marker indicates the average of the data, whereas the upper and lower sides of the boxes indicate the 75 and 25 percentile of the data, respectively.

3.2.2 Diurnal variability

The diurnal variability in $\kappa_{H\text{-}TDMA\_90\%}$ was found different for nucleation ($\kappa_{20nm\_90\%}$), Aitken ($\kappa_{50nm\_90\%}$), and Accumulation ($\kappa_{100nm\_90\%}$, $\kappa_{150nm\_90\%}$, and $\kappa_{200nm\_90\%}$) mode particles. Figure 4 displayed a diel variation of an average of hourly-resolved κ for each size. The bigger size particles exhibited higher values of κ than smaller size

https://doi.org/10.5194/egusphere-2023-577
Preprint. Discussion started: 7 July 2023

particles, which is a similar trend reported at Kanpur, India (Mandariya et al., 2020a) and other worldwide locations (Fan et al., 2020; Hong et al., 2015). In general, it was observed that all size particles exhibited late-night hump (02:00-05:00 hr) in $\kappa_{\text{H-TDMA\_90\%}}$. Besides, only $\kappa_{\text{20nm\_90\%}}$ demonstrated a clear diurnal variability with two peaks, one late night (02:00-04:00 hr) and the other in noontime (14:00-16:00 hr), and two valleys during the morning (07:00-10:00 hr) and night (19:00-22:00 hr). These valleys reflects the strong impacts of local burning and traffic activities (Pringle et al., 2010). In addition, nucleation size particles were potentially contributed by nearly hydrophobic particles (HGF<1.2) from evening to midnight. They showed mono modal GF-PDF around unit hygroscopic growth factor, possibly indicating local emission generated particles. The 20 nm particles are small enough and lie on the boundary of nucleation mode particles. Achtert et al. (2009) reported a similar diurnal trend of Nucleation and Aitken mode particles, attributed the lower values to the emission of hydrophobic aerosol particles during the local burning emissions. Daytime hump is attributed to the intense photochemical oxidation process, which causes the enhancement of more oxidized species on the aerosol particle. Furthermore, their chemical composition is dominantly controlled by the gaseous condensation of H_2SO_4, HNO_3, and VOCs (Hong et al., 2015). The aerosol's chemical composition can address this variability of $\kappa_{\text{H-TDMA\_90\%}}$. However, $\kappa_{\text{50nm\_90\%}}$ also follows a similar diurnal variability as $\kappa_{\text{20nm\_90\%}}$, although it showed less variability. Further, as the dry size of the aerosol particles increased to accumulated mode, diurnal variation shifted toward nearly steady for the rest of the day. Hong et al. (2018) also observed no obvious diurnal pattern for 100 and 150 nm particles of organic-dominated aerosols over the Pearl River Delta region in China.

Furthermore, the diurnal cycles of aerosol physicochemical properties also reflect the dynamic diurnal variation in the planetary boundary layer (PBL) that leads to the accumulation of particles during night-time. Although this study did not quantify size-resolved chemical composition, so, this study used bulk-aerosol composition to address the trend variability only. However, daily average aerosol PNSD varied between 18.0-140.0 nm with a mean of 73.1 ± 33.8 nm. And, the mode of PVSD changed approximately around 300-600 nm. Therefore, it could be an excellent approximation to discuss $\kappa_{\text{200nm\_90\%}}$ variability with aerosol's bulk chemical properties. The midnight to early morning hump in hygroscopicity of accumulation mode particles can be attributed to the high rise in the ratio of inorganic volume fraction to OA volume fraction (Fan et al., 2020), as illustrated in figure 2 (r, s t, u, and v). Moreover, during mid-night and early morning in the winter, water-soluble organic and inorganic gases are partitioned and/or coagulated/condensed on the surface of the pre-existing particles. Further, in the presence of high RH and lower temperature, primary and secondary less oxidized organic aerosol participated in the aging process, which leads to enhancement their oxidation via aqueous/heterogeneous reaction, according to it increase

https://doi.org/10.5194/egusphere-2023-577
Preprint. Discussion started: 7 July 2023

the particle's hygroscopicity (Jimenez et al., 2009; Wu et al., 2016). Similar results were observed by Fan et al. (2020) during winter in urban Beijing, and they attributed it with the enhancement of more hygroscopic particles due to the aqueous-oxidation and/or condensation process on the pre-existing particles. In general, higher noontime solar radiation favors more intense photooxidation processes. It supports the partitioning of relatively more oxidized and less volatile organics on the particulate surface, enhancing the hygroscopicity of accumulation mode particles (Duplissy et al., 2011; Massoli et al., 2010; Tritscher et al., 2011). However, interestingly, we observed a noontime flatten pattern of $\kappa_{H\text{-}TDMA\_90\%,}$ and it could be attributed to the mix of the positive and negative impact of an enhancement in the volume fraction of OA and more hygroscopic ammonium sulfate and decrement in ACl, and AN's volume fraction. Lower volume fractional contribution of highly volatile ACl could be the potential factor that modulates accumulation mode particle's hygroscopicity. This can be supported by the strong correlation of $\kappa_{H\text{-}TDMA\_90\%}$ and volume fraction of ACl in that size particles (ε_{ACl}).

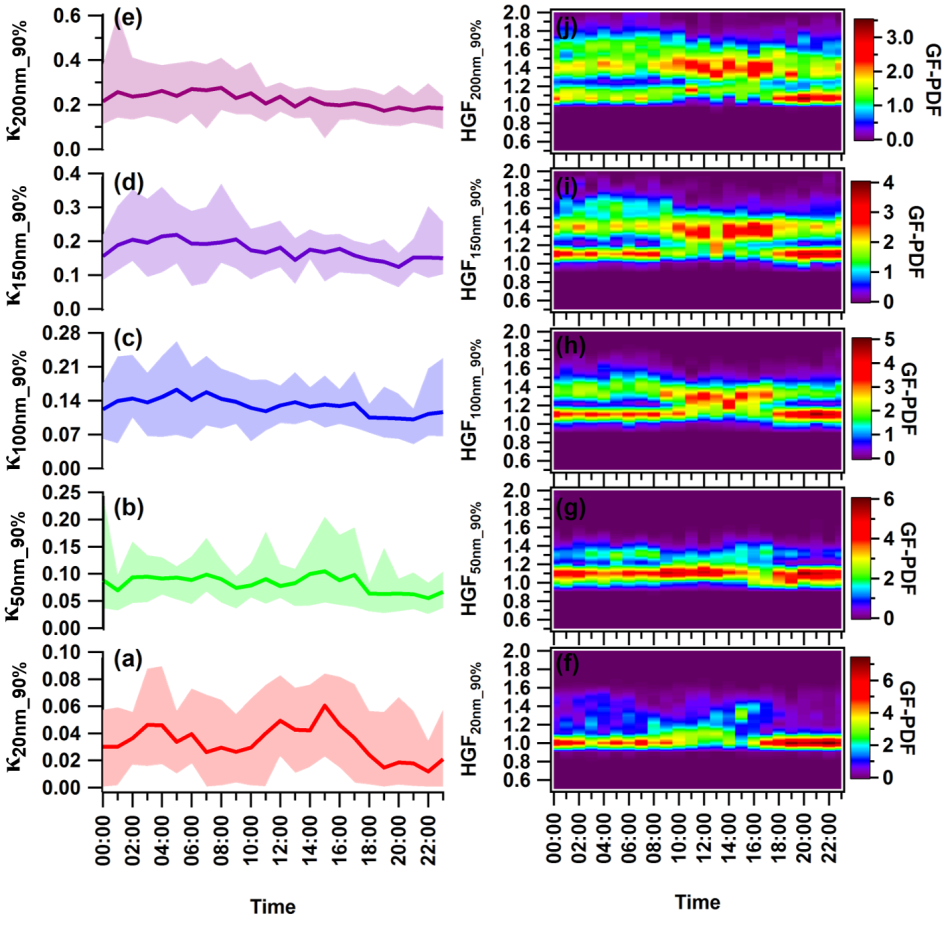

https://doi.org/10.5194/egusphere-2023-577
Preprint. Discussion started: 7 July 2023

Figure 4: Diurnal variance in the hygroscopic parameter kappa (κ) of nucleation mode particles (a) 20 nm ($\kappa_{20nm\_90\%}$), Aitken mode particles (b) 50 nm ($\kappa_{50nm\_90\%}$), and Accumulation mode particles (c) 100 nm ($\kappa_{100nm\_90\%}$), (d) 150 nm ($\kappa_{150nm\_90\%}$), and (e) 200 nm ($\kappa_{200nm\_90\%}$) and hygroscopic growth factor of (f) 20 nm ($HGF_{20nm\_90\%}$), (g) 50 nm ($HGF_{50nm\_90\%}$), (h) 100 nm ($HGF_{200nm\_90\%}$), (i) 150 nm ($HGF_{150nm\_90\%}$), and 200 nm ($\kappa_{200nm\_90\%}$) aerosol particles. The solid line represents diurnal average values, and the upper and lower shaded area represents 95 and 5 percentile values of corresponding average values. Different color coding has been used to represent various size-specific kappa values. The color scale represents the growth factor probability density function of hygroscopic growth factor.

3.2.3 Driving Factor of Hygroscopicity

A correlation analysis was carried out between measured chemical species and aerosol to explore the factors governing aerosol hygroscopicity, as shown in the figure 5. Organic aerosol was observed negatively impact κ, explained by a negative correlation (figure S7(a)). This negative correlation of OA with κ is also observed in India (Bhattu et al., 2016; Mandariya et al., 2020b) and worldwide (Enroth et al., 2018; Hong et al., 2014; Kawana et al., 2016; Kitamori et al., 2009; Wang et al., 2018a; Wu et al., 2013a). This result indicates that primary constituents dominated the OA during high loading, considered nearly hydrophobic or less hygroscopic. In addition, the current study observed that an enhancement of 10% of OA by volume in 200 nm aerosol particles would be responsible for a 4% decrement in its hygroscopicity (figure S7(a)). Interestingly, ammonium sulfate and nitrate showed a positive but poor correlation with hygroscopicity. It could be due to sulfate and nitrate aerosol dominating the bigger particles (>200nm). However, a 10% enhancement of AS by volume was found to be responsible for the enhancement of hygroscopicity only by 1.6%. Besides, figure 5(a) shown an increasing volume fraction of ACl in PM_1 with an increase in aerosol hygroscopicity, and this strong positive correlation is responsible for an enhancement in kappa by 4.2% over the increment of 10% ACl by volume, which was the highest among all chemical species. Further, ammonium chloride has a more significant water uptake potential (Chen et al., 2022; Zhao et al., 2020), which can be justified by the solid correlation of ALWC with a mass fraction of ACl in PM_1 as shown in figure 5(b). This indicates that particles with a more considerable ammonium chloride fraction uptake more water vapor, leading to higher hygroscopic aerosol particles. It is clear that the increases in ammonium chloride fraction enhanced aerosol liquid water content and led to higher hygroscopicity of aerosol particles. A Recent study in Delhi by Chen et al. (2022) unveils that ammonium chloride fraction in PM_1 aerosol enormously enhances during the higher relative humidity conditions during the winter season due to the co-condensation of semivolatile ammonium chloride with water vapor on the particles and leads to enhance water uptake and lead severe winter haze in Delhi. The very high volume fractions (>30%) of ACl in atmospheric NR-

https://doi.org/10.5194/egusphere-2023-577
Preprint. Discussion started: 7 July 2023

PM_1 were observed episodic, suggesting a high fraction of Cl in the particle phase is strongly dependent on excess ammonia in the atmosphere. These results indicate that ammonia is the controlling factor for chloride partitioning in the particle phase, resulting in high aerosol water content under high RH and lower temperature conditions. As the ACl is strongly dependent on the RH and temperature.

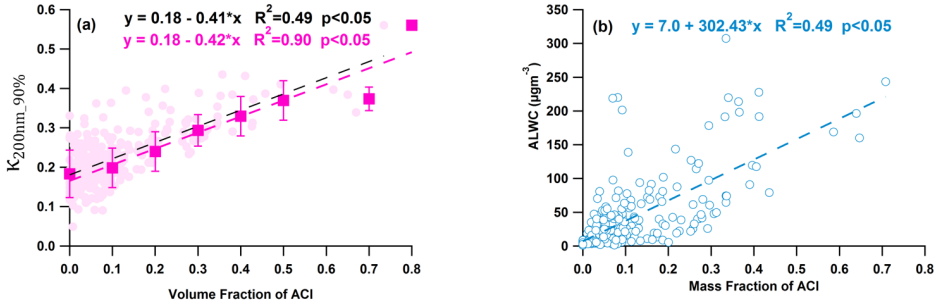

Figure 5: Correlation plot for (a) $\kappa_{200nm\_90\%}$ vs volume fraction of ammonium chloride aerosol (VF_{ACl}) and (b) aerosol liquid water content (ALWC) vs mass fraction of ammonium chloride (MF_{ACl}).

3.2.4 Hygroscopicity during high biomass burning (H-BB), high-hydrocarbon like OA (H-HOA), high-Cl (H-Cl), and Clean Periods

Delhi's atmosphere is a complex array of chloride and organic aerosol sources like combustion (crop residue, agriculture waste, medical waste, municipal waste, plastic, etc., burning) and industrial sources. Therefore, all episodic events were classified into three to investigate the impact of chloride and OA on aerosol hygroscopicity. First, high biomass burning (H-BB) event; second, high-hydrocarbon like OA (H-HOA) event; and third, high-Cl (H-Cl) event according to the substantial fractional contribution of their markers in respective periods. In addition, we also classified a "Clean Period" where PM_1 loading was less than 25 percentile ($\leq 38.7\ \mu gm^{-3}$) of the sampling period. Further, aerosol chemical composition data were filtered according to hygroscopic parameter data for further analysis. By performing so, data information that is characteristic of the local emission and atmospheric chemistry in question and the effects of various potential transported air mass types can be retrieved. It is valuable to extract any possible information about aerosol sources and transformation process evaluation to interpret its influence on the aerosol's hygroscopicity.

3.2.4.1 Relatively Clean Period

https://doi.org/10.5194/egusphere-2023-577
Preprint. Discussion started: 7 July 2023

The relatively Clean period was predominantly dominated by E, S-E winds; however, pollution was associated with calm winds, as illustrated in figure S9. All BBOA, HOA, and ACl were observed to be associated with similar sources and found an excellent association with ambient relative humidity. The mean concentration of organic aerosol, ACl, AN, and AS was observed at 11.0 ± 6.4, 1.4 ± 1.1, 3.0 ± 1.5, and 4.4 ± 2.2 μgm^{-3}, respectively. These mass concentrations were significantly lower than in other specified periods. However, OA was still the dominant species, with 56% by volume in the PM_1, as indicated in figure 8. Among all OA factors, HOA was predominantly dominated in OA with 33%, although secondary organic aerosol confined the overall 54.4% of OA. Secondary OA is defined with relatively higher oxidized OA, and the oxidation state of OA positively impacts OA hygroscopicity (Kim et al., 2017; Richard et al., 2011; Wu et al., 2013a). The Clean period's mean hygroscopicity of 20, 50, 100, 150, and 200 nm particles were observed at 0.03 ± 0.02, 0.09 ± 0.04, 0.14 ± 0.06, 0.22 ± 0.09, and 0.27 ± 0.07, respectively, significantly ($p<0.05$) different to each other. However, the accumulation particle's (200 nm) hygroscopicity was not significantly ($p>0.05$) higher than the 150 nm particles. The hygroscopicity increment with size from 20 to 200 nm can also be explained by the fractional increment of more hygroscopic (GF>1.2) particles relative to nearly hydrophobic or less hygroscopic particles (GF<1.2). Nucleation particles, 20 nm was dominated mostly by less hygroscopic particles (76.8 ± 21.7%), indicates influence by fresh emission sources, whereas, Aitken (50 nm) and Accumulation (200 nm) size aerosol were confined with 69.3 ± 14.7 and 25.4 ± 10.8 less hygroscopic particles, respectively. These results point out that accumulation-size aerosols dominated secondary aerosols, which can also supports their GF-PDF as shown in figure 7(a). Nucleation size aerosol particles (20nm) showed nearly mono modal GF-PDF with the mode of unit growth factor. In contrast, the mode shifted towards the higher end as aerosol size increased and GF-PDF shifted from unit to multi-mode.

3.2.4.2 High-Cl (H-Cl) events

H-Cl events representing the substantial loading of ACl on the receptor site, as shown in the pie chart in figure 8, were chosen mainly due to the significant jump (>20%) in fractional volume contribution NH_4Cl (ε_{ACl}) in the PM_1 aerosol. This period observed apparent surface wind from W-direction, although WNW, WSW, and SE winds also influence the site, as shown in figure 6(b). BBOA and HOA are potentially contributed from the WNW and SE directions, as explained in the bipolar plot figure 6(c & d), and seem to come from a similar local source. Among inorganic species, ACl observed excellent association with ambient RH, as shown in figure 6(e) and (f), indicating the atmospheric gaseous HCl neutralized with NH_3 gas in the presence of atmospheric water content. HCl sources could be coal power plants, trash burnings in solid waste dumping sites, and other industries located

https://doi.org/10.5194/egusphere-2023-577
Preprint. Discussion started: 7 July 2023

in the W-WSW direction (Gani et al., 2019), as shown in the map in figure 6(a). Atmospheric high Cl events are potentially dominated by trash burning in Delhi during winter (Shukla et al., 2021; Tobler et al., 2020). Moreover, bipolar plots (figure 6(e and f)) suggest that ACl formation under high RH conditions associated with a relatively calm atmosphere trigger particles' hygroscopicity. This hypothesis can be supported with a good association of aerosol liquid water content (ALWC) as discussed in previous section. Furthermore, GF-PDF of all size particle marked relatively more fractionaly contribution of secondary mode particles as showed in figure 7(d). Overall more hygroscopic (HGF90%>1.2) particles were marked by 42, 47, 50, 74, and 83% contributions in the 20, 50, 100, 150, and 200 nm size particles, respectively. Hence, ACl is a critical factor to enhance aerosol hygroscopicity to trigger fog/haze formation under higher RH and colder atmospheric conditions as discussed in the previous section.

Similarly, Gunthe et al. (2021) observed that high local emission of hydrochloric acid in Delhi during February-March gets partitions into aerosol liquid water under high humid conditions, enhancing the water uptake capacity of aerosol sustain particle's hygroscopic growth, result in fog/haze formation. Moreover, worldwide studies on size-resolved hygroscopicity observed Cl less than 1%, so they omitted ACl as an aerosol constituent into the discussion. In addition, the current study did not find any strong correlation of κ with AS and AN. It could be due to their association with larger particle sizes. Besides, ACl could be associated with comparatively lower size particles ($\leq$ 200 nm). Furthermore, in context to look influence of air mass trajectories, we further mapped aerosol's constituents in the association of air mass back trajectories in PSCF to see the potential area source contribution influencing the aerosol evaluation processes, ultimately aerosol's hygroscopicity. However, we did not find any back trajectory influencing the receptor site, as all trajectory endpoints were observed above the planetary boundary layer height.

https://doi.org/10.5194/egusphere-2023-577
Preprint. Discussion started: 7 July 2023

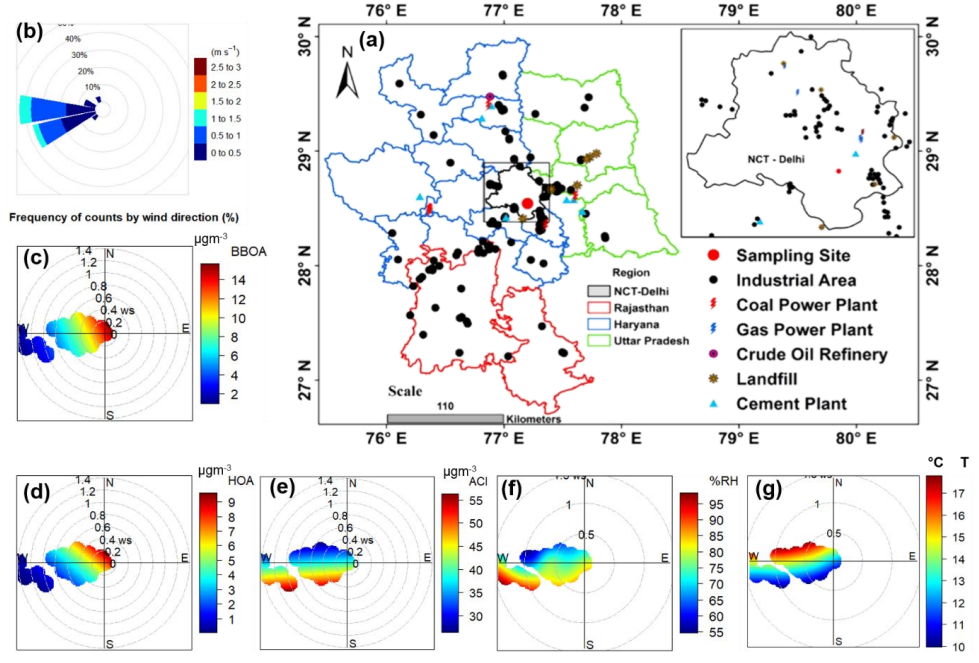

Figure 6: Map of (a) Delhi showing various types of industries located in the region and nearby locations, (b) wind rose diagram and conditional bi-polar plots showing variation in mass concentration of (c) biomass burning OA (BBOA), (d) hydrocarbon like OA (HOA), (e) ammonium chloride (ACl), (f) % ambient relative humidity (RH), and (g) ambient temperature (T), with wind direction (WD) and wind speed (WS) during H-Cl events. A background map showing various industrial locations was adapted from Rai et al. (2020).

3.2.4.3 High biomass burning (H-BB) Events

High BB periods were noted during the initial period (1-12 February) of the field campaign. The predominant surface wind circulations were from W, W-WNW, and W-WSW directions (figure S8(b)). The aerosol was dominated by local emissions, as aerosol constituents are mainly associated with slower wind circulations from landfill sites, industrial areas, and coal power plants, as shown in figure S8(a). Further, it could justify the potential source contribution function (PSCF) analysis considering 48-hr air mass back trajectories, as shown in figure S10. Therefore, BBOA possibly contributed from the open local biomass burning activities at landfill sites or others. Biomass burning organic aerosol confined the most considerable fraction, 39%, of organic aerosol, following HOA, 28%. Figure S5(b, c, and d) clearly shows that BBOA and HOA have similar source profiles but differ from the ACl source. Moreover, ACl was not found to have a good association with ambient RH and but was associated with nearby coal power plant's emissions. However, 48 h air mass back trajectories indicated that the current city

https://doi.org/10.5194/egusphere-2023-577
Preprint. Discussion started: 7 July 2023

was also influenced by air mass from some parts of Uttar Pradesh, Punjab, and Haryana. These states are the potential hub of crop residue burning, industrial activities and brick kilns. These cities have a substantial fraction of OA in PM_1 and OA mainly affected by biomass activities during winter. The H-BB event captured a considerable volume fraction, 71% of OA in PM_1 and BBOA contributed almost 39%, as illustrated in the figure 8. So, lower inorganic to OA ratio was a potential factor in decreasing the aerosol hygroscopicity in H-BB events. Further, a primary organic aerosol contribution was enhanced during this event and, on average, raised to 67%. OA loading inversely affects the aerosol's hygroscopicity. Mandariya et al. (2020) reported a similar observation in Kanpur, and the authors suggested that the contribution of primary biomass burning (BBOA) and hydrocarbon-like OA adversely affects aerosol hygroscopicity. BBOA showed a good negative correlation with the hygroscopicity of 200 nm particles, supporting the following conclusion. Apart from this, the Nucleation size particle (20 nm) showed 0.02 ± 0.02 hygroscopicity parameter with mono mode GF-PDF with the unit mode (figure 7(b)) and confined 83.7 ± 18.6 % nearly hydrophobic particles. Furthermore, as aerosol size increased, hygroscopicity parameter ($\kappa_{H\text{-}TDMA\_90\%}$) enhanced significantly ($p<0.05$) as the contribution of relatively secondary aerosol particles (GF>1.2) increased with aerosol size. Accumulation size aerosol, 100 nm contributed approximately 54% by nearly hydrophobic (GF<1.2) and 46% by more hygroscopic (GF>1.2) particles.

3.2.4.4 High-HOA (H-HOA) Events

H-HOA events were identified based on the considerable mass concentration and fraction of HOA in the organic aerosol. These periods were noted generally 19:00 hr to Morning 09:00 hr during 22-23 and 26-27 February and 4, and 7-8 March as indicated in figure 1. PSCF explore the probability of impacts of long-range transported aerosol. Interestingly, it was observed that air masses over Delhi, Haryana, and Uttar Pradesh were potentially associated with hydrocarbon-like OA (figure S10). BBOA also followed a similar path as HOA. However, the potential area source of ACl was the nearby region of Delhi and Haryana. The HOA loading was significantly ($p<0.05$) higher than in H-BB, H-Cl and Clean periods. However, emission sources were different during both H-HOA and H-BB periods. As HOA was the potential contributor to OA, it is likely the critical constituent to modulate aerosol hygroscopicity in the region during these events. HOA is mainly considered hydrophobic (Duplissy et al., 2011). Therefore, elevated HOA contribution (41%) in OA could be responsible for lower κ in these events. The overall hygroscopicity of 20, 50, 100, 150, and 200 nm size particles was recorded as 0.01 ± 0.01, 0.06 ± 0.03, 0.11 ± 0.03, 0.14 ± 0.04, and 0.17 ± 0.05, respectively. The predominant fractional contribution of primary aerosol particles (GF<1.2) seems to be a reason for this lower hygroscopicity of particles, as shown in figure 7(c). Overall, OA predominantly constitutes the fraction in the PM_1, and primary OA contributed

https://doi.org/10.5194/egusphere-2023-577
Preprint. Discussion started: 7 July 2023

approximately 60% in OA. However, relative increment in the contribution of other more hygroscopic constituents like secondary organic aerosol (LO-OOA and MO-OOA), ACl and ammonium sulfate (AS) in the aerosol possible tried to balance the negative impact high-HOA on which limited κ.

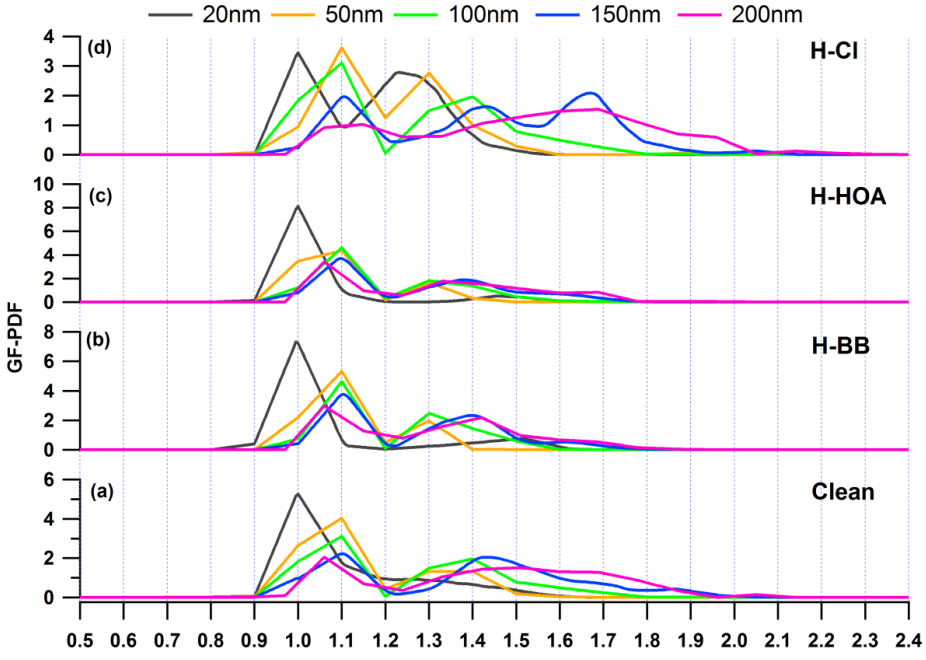

Figure 7: Growth Factor Probability Density Function (GF-PDF) of 20, 50, 100, 150, and 200 nm aerosol particles for the (a) clean, (b) H-BB, (c) H-HOA, and H-Cl periods.

3.2.4.4 Comparison of κ of different events

We choose a 200 nm accumulation particle size particle representing the bulk aerosol chemical composition to compare the aerosol hygroscopicity among various periods. Further, in the present study, the mode of particle-volume size distribution varied from 400 nm to 600 nm particle dry mobility diameter. Therefore, 200 nm size accumulation particles are the best choice to compare hygroscopicity parameters among different periods considering bulk aerosol composition in various mentioned periods. In addition, a good Pearson's r value, 0.76, was found among $\kappa_{200nm\_90\%}$ and $\kappa_{chem\_90\%}$, derived from the dry PM_1 particle's chemical composition measured from the ACSM based on the ZSR mixing rule (Stokes and Robinson, 1966), which justifies our choice.

https://doi.org/10.5194/egusphere-2023-577
Preprint. Discussion started: 7 July 2023

The H-Cl event noted the highest value (0.36 ± 0.06) of $\kappa_{200nm\_90\%}$ against H-BB (0.18 ± 0.04), H-HOA (0.17 ± 0.05), and Clean (0.27 ± 0.07) events, as illustrated in figure 8. The H-Cl event observed that the average $\kappa_{200nm\_90\%}$ value was significantly ($p<0.05$) higher than those observed in other events. It means that a substantial increment in Cl emission in the Delhi region could significantly enhance the aerosol liquid water content leading to higher aerosol hygroscopicity, which can further strengthen cloud condensation nuclei formation, possibly triggering haze/fog events in Delhi NCR (Gunthe et al., 2021). These results suggest that controlling the open trash/waste burning in the region could help control Cl emission, which leads to minimizing the haze/fog formation possibility during high atmospheric conditions. However, the difference in $\kappa_{200nm\_90\%}$ values between H-BB and H-HOA events was not observed significantly ($p>0.05$), possibly due to the relative changes in primary, secondary OA, and inorganic species. In the H-HOA events, the negative effect of a significantly higher fractional (41%) contribution of HOA to OA possibly balances with a positive impact of a 7% increment in secondary OA relative to H-BB. Worldwide studies (Jimenez et al., 2009; Mandariya et al., 2019; Sun et al., 2013) reported secondary organic aerosol associated with a higher O/C ratio, and several studies reported that the O/C ratio positively correlated to κ (Jimenez et al., 2009; Kim et al., 2020) as described in the earlier text. Furthermore, impacts of 5% decrement in ACl during H-HOA event concerning H-BB event possibly managed by 7% increment in AS fraction. Overall, these relative changes in aerosol constituents worked to insignificant changes in κ during H-BB and H-HOA periods. Nevertheless, H-BB and H-HOA events witnessed significant ($p<0.05$) lower hygroscopicity compared to a relatively cleaner atmosphere. The aerosol associated with relatively cleaner events was with a higher inorganic-to-organic ratio. In addition, the aerosol in clean periods comprised a significantly higher fraction of secondary organic aerosol, which could be the reason for the higher hygroscopicity associated with organic aerosol compared to other events. Worldwide (Aiken et al., 2008; Cerully et al., 2015b; Chakraborty et al., 2016b; Mandariya et al., 2019) studies have reported that organic aerosol loading inversely impacts the oxidation/aging process of OA. Overall, all these were responsible for higher hygroscopicity in relatively cleaner periods.

https://doi.org/10.5194/egusphere-2023-577
Preprint. Discussion started: 7 July 2023

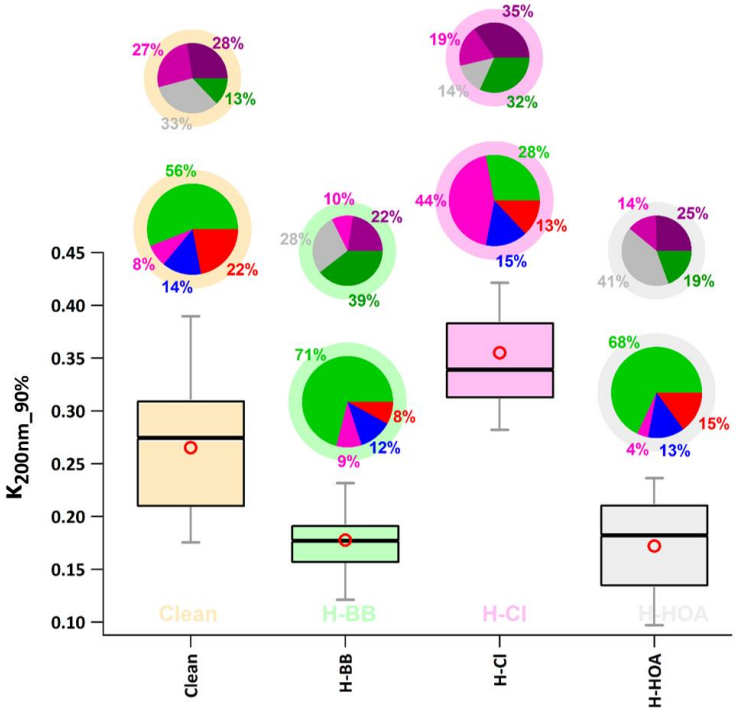

Figure 8: Box plot showing variation in H-TDMA measured hygroscopic parameter of 200 nm size particles $\kappa_{H\text{-}TDMA}$ ($\kappa_{200nm\_90\%}$) in high biomass burning (H-BB), high-chloride (H-Cl), and high-hydrocarbon like organic aerosol (H-HOA) events. Different colors represent respective events in the plot. A bigger pie chart represents the overall average volume fractional contribution of various aerosol species indicated by color-coding. In addition, minor pie charts described the event average mass fractional contribution of different OA species in OA. Diffused ring color of the pie chart displays the respective event.

4. Conclusions

The current study explored the temporal variation of Nucleation (20 nm), Aitken (50 nm), and Accumulation (150 and 200 nm) mode particle hygroscopicity in Delhi during the winter period, February-March 2020. In addition, the present study highlighted the hygroscopicity variation in relatively higher chloride, biomass burning, and hydrocarbon-like organic aerosol. Because, Delhi highlighted as one of the most polluted cities, faces high chloride pollution episodes during winter haze/fog. Therefore, we reported temporal variation in the size-resolved hygroscopic parameter ($\kappa_{H\text{-}TDMA\_90\%}$) at the sub-saturated level (90% RH) for the first time in Delhi. However, we reported hygroscopicity of nucleation and Aitken mode particles for the first time in India.

https://doi.org/10.5194/egusphere-2023-577
Preprint. Discussion started: 7 July 2023

The observed $\kappa_{H\text{-}TDMA\_90\%}$ ranged from .00 to 0.11 (0.03 ± 0.02), 0.05 to 0.22 (0.11 ± 0.03), 0.05 to 0.30 (0.14 ± 0.04), 0.05 to 0.41 (0.18 ± 0.06), and 0.05 to 0.56 (0.22 ± 0.07) for 20, 50, 100, 150, and 200 nm aerosol particles, respectively. The study period's mean value of the hygroscopicity parameter was significantly ($p<0.05$) enhanced with the size of the particles. $\kappa_{20nm\_90\%}$ and $\kappa_{50nm\_90\%}$ were observed to show dynamic diurnal variation. In contrast, as particle size increased in accumulation mode particles, noontime variation became flatten, which found an attribute with neutralizing positive and negative impacts of increment and decrement in volume fraction of NH_4Cl and OA, respectively. Interestingly, the variation in $\kappa_{200nm\_90\%}$ was observed potentially due to variation in NH_4Cl and OA instead $(NH_4)_2SO_4$.

Furthermore, the pollution episodes were generally associated with local biomass burning and industrial and waste-burning emissions in Delhi and nearby regions. We mainly focused on emphasizing the impacts of high biomass burning (H-BB), high hydrocarbons like OA (H-HOA), and high chloride emission (H-Cl) on aerosol hygroscopicity and their relative comparison with the cleaner period. The H-Cl period was observed significantly ($p<0.05$) higher hygroscopicity (0.35 ± 0.06) compared to H-BB (0.18 ± 0.04), H-HOA (0.17 ± 0.05), and relatively cleaner period (0.27 ± 0.07). However, H-BB and H-HOA showed no significant difference in hygroscopicity. However, they witnessed lower aerosol hygroscopicity concerning a relatively cleaner atmosphere. It could be attributed to the lower organic aerosol loading and higher inorganic-to-organic aerosol ratio in the aerosol. High atmospheric chloride aerosol (ammonium chloride) was observed most affectionately to the atmospheric water, leading to higher aerosol liquid water content at high chloride events. In addition, a high volume fraction of ammonium chloride in aerosol enhanced the aerosol hygroscopic nature. Furthermore, our results based on episodic interpretation revealed that chloride emission is a significant concern in Delhi, which enhances the aerosol's hygroscopicity, helps to act as CCN to form fog droplets during winter colder days, and leads to fog/haze formation in Delhi. In addition, high chloride present in aerosol overcomes the negative impact of high OA loading on CCN activity. Hence, our results suggest controlling waste materials' open burning to decrease the haze/fog events in Delhi during winter.

Supporting Information

Supplementary pieces of information are mentioned in the supplementary file.

Data availability. Data can be accessed at the following repository:

https://web.iitd.ac.in/~gazala/publications.html (Mandariya et al., 2023).

https://doi.org/10.5194/egusphere-2023-577
Preprint. Discussion started: 7 July 2023

Author contributions

AH, MMVH, NAB, and GH operated aerosol instrumentation and collection of data on-board in Delhi. KP analysed the ACSM data. AKM, AH, and GH conceptualized the structure of the manuscript. AKM analysed, evaluated H-TDMA data, and wrote the manuscript. AH analysed MPSS data. AKM, AH, KP, JSA, LHR, AW, and GH internally reviewed the manuscript and helped to write the manuscript.

Corresponding Author

Gazala Habib (gazalahabib@civil.iitd.ac.in) and Alfred Wiedensohler (ali@tropos.de)

Competing interests

The authors declare that they have no conflict of interest.

Acknowledgment

The authors thankful to Dr. Martin Gysel, Aerosol Physics Group, Paul Scherrer Institute, Switzerland, for providing TDMAinv toolkit for HTDMA data correction.

REFERENCES

Achtert, P., Birmili, W., Nowak, A., Wehner, B., Wiedensohler, A., Takegawa, N., Kondo, Y., Miyazaki, Y., Hu, M. and Zhu, T.: Hygroscopic growth of tropospheric particle number size distributions over the North China Plain, J. Geophys. Res., 114(8), D00G07, doi:10.1029/2008JD010921, 2009.

Aiken, A. C., Decarlo, P. F., Kroll, J. H., Worsnop, D. R., Huffman, J. A., Docherty, K. S., Ulbrich, I. M., Mohr, C., Kimmel, J. R., Sueper, D., Sun, Y., Zhang, Q., Trimborn, A., Northway, M., Ziemann, P. J., Canagaratna, M. R., Onasch, T. B., Alfarra, M. R., Prevot, A. S. H., Dommen, J., Duplissy, J., Metzger, A., Baltensperger, U. and Jimenez, J. L.: O/C and OM/OC ratios of primary, secondary, and ambient organic aerosols with high-resolution time-of-flight aerosol mass spectrometry, Environ. Sci. Technol., 42(12), 4478–4485, doi:10.1021/es703009q, 2008.

Albrecht, B. A.: Aerosols, Cloud Microphysics, and Fractional Cloudiness, Science (80-.)., 245(4923), 1227–1230, doi:10.1126/science.245.4923.1227, 1989.

Arub, Z., Bhandari, S., Gani, S., Apte, J. S., Hildebrandt Ruiz, L. and Habib, G.: Air mass physiochemical characteristics over New Delhi: impacts on aerosol hygroscopicity and cloud condensation nuclei (CCN) formation, Atmos. Chem. Phys., 20(11), 6953–6971, doi:10.5194/acp-20-6953-2020, 2020.

Bhandari, S., Gani, S., Patel, K., Wang, D. S., Soni, P., Arub, Z., Habib, G., Apte, J. S. and Hildebrandt Ruiz, L.: Sources and atmospheric dynamics of organic aerosol in New Delhi, India: insights from receptor modeling, Atmos. Chem. Phys., 20(2), 735–752, doi:10.5194/acp-20-735-2020, 2020.

Bhattu, D. and Tripathi, S. N.: CCN closure study: Effects of aerosol chemical composition andmixing state, J. Geophys. Res., 120(2), 766–783, doi:10.1002/2014JD021978, 2015.

Bhattu, D., Tripathi, S. N. and Chakraborty, A.: Deriving aerosol hygroscopic mixing state from size-resolved CCN activity and HR-ToF-AMS measurements, Atmos. Environ., 142, 57–70,

https://doi.org/10.5194/egusphere-2023-577
Preprint. Discussion started: 7 July 2023

doi:10.1016/j.atmosenv.2016.07.032, 2016.

Cerully, K. M., Bougiatioti, A., Hite, J. R., Guo, H., Xu, L., Ng, N. L., Weber, R. and Nenes, A.: On the link between hygroscopicity, volatility, and oxidation state of ambient and water-soluble aerosols in the southeastern United States, Atmos. Chem. Phys., 15(15), 8679–8694, doi:10.5194/acp-15-8679-2015, 2015a.

Cerully, K. M., Bougiatioti, A., Hite, J. R., Guo, H., Xu, L., Ng, N. L., Weber, R. and Nenes, A.: On the link between hygroscopicity, volatility, and oxidation state of ambient and water-soluble aerosols in the southeastern United States, Atmos. Chem. Phys., 15(15), 8679–8694, doi:10.5194/acp-15-8679-2015, 2015b.

Chakraborty, A., Gupta, T. and Tripathi, S. N.: Combined effects of organic aerosol loading and fog processing on organic aerosols oxidation, composition, and evolution, Sci. Total Environ., 573, 690–698, doi:10.1016/j.scitotenv.2016.08.156, 2016a.

Chakraborty, A., Gupta, T. and Tripathi, S. N.: Combined effects of organic aerosol loading and fog processing on organic aerosols oxidation, composition, and evolution, Sci. Total Environ., 573, 690–698, doi:10.1016/j.scitotenv.2016.08.156, 2016b.

Chen, Y., Wang, Y., Nenes, A., Wild, O., Song, S., Hu, D., Liu, D., He, J., Hildebrandt Ruiz, L., Apte, J. S., Gunthe, S. S. and Liu, P.: Ammonium Chloride Associated Aerosol Liquid Water Enhances Haze in Delhi, India, Environ. Sci. Technol., 56(11), 7163–7173, doi:10.1021/ACS.EST.2C00650, 2022.

Draxler, Roland R., Hess, G. D.: Descrpition of the HYSPLIT_4 Modeling System, NOAA Techincal Memo. ERL ARL-224, (October 2004), 28 [online] Available from: http://arlsun.arlhq.noaa.gov/documents/reports/arl-224.pdf%5Cnhttp://www.ciecem.uhu.es/hysplitweb08/document/arl-224.pdf, 1997.

Duplissy, J., De Carlo, P. F., Dommen, J., Alfarra, M. R., Metzger, A., Barmpadimos, I., Prevot, A. S. H., Weingartner, E., Tritscher, T., Gysel, M., Aiken, A. C., Jimenez, J. L., Canagaratna, M. R., Worsnop, D. R., Collins, D. R., Tomlinson, J. and Baltensperger, U.: Relating hygroscopicity and composition of organic aerosol particulate matter, Atmos. Chem. Phys., 11(3), 1155–1165, doi:10.5194/acp-11-1155-2011, 2011.

Enroth, J., Mikkilä, J., Németh, Z., Kulmala, M. and Salma, I.: Wintertime hygroscopicity and volatility of ambient urban aerosol particles, Atmos. Chem. Phys., 18(7), 4533–4548, doi:10.5194/acp-18-4533-2018, 2018.

Ervens, B., Turpin, B. J. and Weber, R. J.: Secondary organic aerosol formation in cloud droplets and aqueous particles (aqSOA): A review of laboratory, field and model studies, Atmos. Chem. Phys., 11(21), 11069–11102, doi:10.5194/acp-11-11069-2011, 2011.

Fan, X., Liu, J., Zhang, F., Chen, L., Collins, D., Xu, W., Jin, X., Ren, J., Wang, Y., Wu, H., Li, S., Sun, Y. and Li, Z.: Contrasting size-resolved hygroscopicity of fine particles derived by HTDMA and HR-ToF-AMS measurements between summer and winter in Beijing: the impacts of aerosol aging and local emissions, Atmos. Chem. Phys., 20(2), 915–929, doi:10.5194/acp-20-915-2020, 2020.

Fountoukis, C. and Nenes, A.: ISORROPIAII: A computationally efficient thermodynamic equilibrium model for K+-Ca2+-Mg2+-NH4+-Na+-SO42--NO3--Cl--H2O aerosols, Atmos. Chem. Phys., 7(17), 4639–4659, doi:10.5194/acp-7-4639-2007, 2007.

Gani, S., Bhandari, S., Seraj, S., Wang, D. S., Patel, K., Soni, P., Arub, Z., Habib, G., Hildebrandt Ruiz, L. and Apte, J. S.: Submicron aerosol composition in the world's most polluted megacity: the Delhi Aerosol Supersite study, Atmos. Chem. Phys., 19(10), 6843–6859, doi:10.5194/acp-19-6843-2019, 2019.

Gunthe, S. S., Rose, D., Su, H., Garland, R. M., Achtert, P., Nowak, A., Wiedensohler, A., Kuwata, M., Takegawa, N., Kondo, Y., Hu, M., Shao, M., Zhu, T., Andreae, M. O. and Pöschl, U.: Cloud condensation nuclei (CCN) from fresh and aged air pollution in the megacity region of Beijing, Atmos. Chem. Phys., 11(21), 11023–11039, doi:10.5194/acp-11-11023-2011, 2011.

Gunthe, S. S., Liu, P., Panda, U., Raj, S. S., Sharma, A., Darbyshire, E., Reyes-Villegas, E., Allan, J., Chen, Y., Wang, X., Song, S., Pöhlker, M. L., Shi, L., Wang, Y., Kommula, S. M., Liu, T., Ravikrishna, R., McFiggans, G., Mickley, L. J., Martin, S. T., Pöschl, U., Andreae, M. O. and Coe, H.: Enhanced aerosol particle growth sustained by high continental chlorine emission in India, Nat. Geosci., 14(2), 77–84, doi:10.1038/s41561-020-00677-x,

https://doi.org/10.5194/egusphere-2023-577
Preprint. Discussion started: 7 July 2023

2021.

Gupta, T. and Mandariya, A.: Sources of submicron aerosol during fog-dominated wintertime at Kanpur, Environ. Sci. Pollut. Res., 20(8), doi:10.1007/s11356-013-1580-6, 2013.

Gysel, M., Crosier, J., Topping, D. O., Whitehead, J. D., Bower, K. N., Cubison, M. J., Williams, P. I., Flynn, M. J., McFiggans, G. B. and Coe, H.: Closure study between chemical composition and hygroscopic growth of aerosol particles during TORCH2, Atmos. Chem. Phys., 7(24), 6131–6144, doi:10.5194/acp-7-6131-2007, 2007.

Gysel, M., McFiggans, G. B. and Coe, H.: Inversion of tandem differential mobility analyser (TDMA) measurements, J. Aerosol Sci., 40(2), 134–151, doi:10.1016/j.jaerosci.2008.07.013, 2009.

Hallquist, M., Wenger, J. C., Baltensperger, U., Rudich, Y., Simpson, D., Claeys, M., Dommen, J., Donahue, N. M., George, C., Goldstein, A. H., Hamilton, J. F., Herrmann, H., Hoffmann, T., Linuma, Y., Jang, M., Jenkin, M. E., Jimenez, J. L., Kiendler-Scharr, A., Maenhaut, W., McFiggans, G., Mentel, T. F., Monod, A., Pŕevôt, A. S. H., Seinfeld, J. H., Surratt, J. D., Szmigielski, R. and Wildt, J.: The formation, properties and impact of secondary organic aerosol: current and emerging issues, Atmos. Chem. Phys., 9(November 2008), 5155–5236, 2009.

Hong, J., Häkkinen, S. A. K., Paramonov, M., Äijälä, M., Hakala, J., Nieminen, T., Mikkilä, J., Prisle, N. L., Kulmala, M., Riipinen, I., Bilde, M., Kerminen, V. M. and Petäjä, T.: Hygroscopicity, CCN and volatility properties of submicron atmospheric aerosol in a boreal forest environment during the summer of 2010, Atmos. Chem. Phys., 14(9), 4733–4748, doi:10.5194/acp-14-4733-2014, 2014.

Hong, J., Kim, J., Nieminen, T., Duplissy, J., Ehn, M., Äijälä, M., Hao, L. Q., Nie, W., Sarnela, N., Prisle, N. L., Kulmala, M., Virtanen, A., Petäjä, T. and Kerminen, V. M.: Relating the hygroscopic properties of submicron aerosol to both gas- and particle-phase chemical composition in a boreal forest environment, Atmos. Chem. Phys., 15(20), 11999–12009, doi:10.5194/acp-15-11999-2015, 2015.

Hong, J., Xu, H., Tan, H., Yin, C., Hao, L., Li, F., Cai, M., Deng, X., Wang, N., Su, H., Cheng, Y., Wang, L., Petäjä, T. and Kerminen, V. M.: Mixing state and particle hygroscopicity of organic-dominated aerosols over the Pearl River Delta region in China, Atmos. Chem. Phys., 18(19), 14079–14094, doi:10.5194/acp-18-14079-2018, 2018.

Hu, D., Chen, J., Ye, X., Li, L. and Yang, X.: Hygroscopicity and evaporation of ammonium chloride and ammonium nitrate: Relative humidity and size effects on the growth factor, Atmos. Environ., 45(14), 2349–2355, doi:10.1016/j.atmosenv.2011.02.024, 2011.

Jimenez, J. L., Canagaratna, M. R., Donahue, N. M., Prevot, A. S. H., Zhang, Q., Kroll, J. H., DeCarlo, P. F., Allan, J. D., Coe, H., Ng, N. L., Aiken, A. C., Docherty, K. S., Ulbrich, I. M., Grieshop, A. P., Robinson, A. L., Duplissy, J., Smith, J. D., Wilson, K. R., Lanz, V. A., Hueglin, C., Sun, Y. L., Tian, J., Laaksonen, A., Raatikainen, T., Rautiainen, J., Vaattovaara, P., Ehn, M., Kulmala, M., Tomlinson, J. M., Collins, D. R., Cubison, M. J., Dunlea, E. J., Huffman, J. A., Onasch, T. B., Alfarra, M. R., Williams, P. I., Bower, K., Kondo, Y., Schneider, J., Drewnick, F., Borrmann, S., Weimer, S., Demerjian, K., Salcedo, D., Cottrell, L., Griffin, R., Takami, A., Miyoshi, T., Hatakeyama, S., Shimono, A., Sun, J. Y., Zhang, Y. M., Dzepina, K., Kimmel, J. R., Sueper, D., Jayne, J. T., Herndon, S. C., Trimborn, A. M., Williams, L. R., Wood, E. C., Middlebrook, A. M., Kolb, C. E., Baltensperger, U. and Worsnop, D. R.: Evolution of organic aerosols in the atmosphere, Science (80-.)., 326(5959), 1525–1529, doi:10.1126/science.1180353, 2009.

Kawana, K., Nakayama, T. and Mochida, M.: Hygroscopicity and CCN activity of atmospheric aerosol particles and their relation to organics: Characteristics of urban aerosols in Nagoya, Japan, J. Geophys. Res. Atmos., 121(8), 4100–4121, doi:10.1002/2015JD023213, 2016.

Kecorius, S., Vogl, T., Paasonen, P., Lampilahti, J., Rothenberg, D., Wex, H., Zeppenfeld, S., Van Pinxteren, M., Hartmann, M., Henning, S., Gong, X., Welti, A., Kulmala, M., Stratmann, F., Herrmann, H. and Wiedensohler, A.: New particle formation and its effect on cloud condensation nuclei abundance in the summer Arctic: a case study in the Fram Strait and Barents Sea, Atmos. Chem. Phys, 19, 14339–14364, doi:10.5194/acp-19-14339-2019, 2019.

Kim, N., Park, M., Yum, S. S., Park, J. S., Song, I. H., Shin, H. J., Ahn, J. Y., Kwak, K. H., Kim, H., Bae, G. N. and Lee, G.: Hygroscopic properties of urban aerosols and their cloud condensation nuclei activities measured in

https://doi.org/10.5194/egusphere-2023-577
Preprint. Discussion started: 7 July 2023

Seoul during the MAPS-Seoul campaign, Atmos. Environ., 153, 217–232, doi:10.1016/j.atmosenv.2017.01.034, 2017.

Kim, N., Yum, S. S., Park, M., Park, J. S., Shin, H. J. and Ahn, J. Y.: Hygroscopicity of urban aerosols and its link to size-resolved chemical composition during spring and summer in Seoul, Korea, Atmos. Chem. Phys., 20(19), 11245–11262, doi:10.5194/acp-20-11245-2020, 2020.

Kitamori, Y., Mochida, M. and Kawamura, K.: Assessment of the aerosol water content in urban atmospheric particles by the hygroscopic growth measurements in Sapporo, Japan, Atmos. Environ., 43(21), 3416–3423, doi:10.1016/j.atmosenv.2009.03.037, 2009.

Kroll, J. H., Donahue, N. M., Jimenez, J. L., Kessler, S. H., Canagaratna, M. R., Wilson, K. R., Altieri, K. E., Mazzoleni, L. R., Wozniak, A. S., Bluhm, H., Mysak, E. R., Smith, J. D., Kolb, C. E. and Worsnop, D. R.: Carbon oxidation state as a metric for describing the chemistry of atmospheric organic aerosol, Nat. Chem., 3(2), 133–139, doi:10.1038/nchem.948, 2011.

Li, H., Wang, Q., Shao, M., Wang, J., Wang, C., Sun, Y., Qian, X., Wu, H., Yang, M. and Li, F.: Fractionation of airborne particulate-bound elements in haze-fog episode and associated health risks in a megacity of southeast China, Environ. Pollut., 208, 655–662, doi:10.1016/j.envpol.2015.10.042, 2016.

Liu, J., Horowitz, L. W., Fan, S., Carlton, A. G. and Levy, H.: Global in-cloud production of secondary organic aerosols: Implementation of a detailed chemical mechanism in the GFDL atmospheric model AM3, J. Geophys. Res. Atmos., 117(D15), n/a-n/a, doi:10.1029/2012JD017838, 2012.

Lohmann, U. and Feichter, J.: Global indirect aerosol effects: a review, Atmos. Chem. Phys., 5(3), 715–737, doi:10.5194/acp-5-715-2005, 2005.

Mandariya, A. K., Gupta, T. and Tripathi, S. N.: Effect of aqueous-phase processing on the formation and evolution of organic aerosol (OA) under different stages of fog life cycles, Atmos. Environ., 206(November 2018), 60–71, doi:10.1016/j.atmosenv.2019.02.047, 2019.

Mandariya, A. K., Tripathi, S. N., Gupta, T. and Mishra, G.: Wintertime hygroscopic growth factors (HGFs) of accumulation mode particles and their linkage to chemical composition in a heavily polluted urban atmosphere of Kanpur at the Centre of IGP, India: Impact of ambient relative humidity, Sci. Total Environ., 704, 135363, doi:10.1016/j.scitotenv.2019.135363, 2020a.

Mandariya, A. K., Tripathi, S. N., Gupta, T. and Mishra, G.: Wintertime hygroscopic growth factors (HGFs) of accumulation mode particles and their linkage to chemical composition in a heavily polluted urban atmosphere of Kanpur at the Centre of IGP, India: Impact of ambient relative humidity, Sci. Total Environ., 704, doi:10.1016/j.scitotenv.2019.135363, 2020b.

Massling, A., Leinert, S., Wiedensohler, A. and Covert, D.: Hygroscopic growth of sub-micrometer and one-micrometer aerosol particles measured during ACE-Asia, Atmos. Chem. Phys, 7, 3249–3259 [online] Available from: www.atmos-chem-phys.net/7/3249/2007/ (Accessed 30 October 2022), 2007.

Maßling, A., Wiedensohler, A., Busch, B., Neusüß, C., Neusüß, N., Quinn, P., Bates, T. and Covert, D.: Atmospheric Chemistry and Physics Hygroscopic properties of different aerosol types over the Atlantic and Indian Oceans, Atmos. Chem. Phys, 3, 1377–1397 [online] Available from: www.atmos-chem-phys.org/acp/3/1377/ (Accessed 30 October 2022), 2003.

Massoli, P., Lambe, A. T., Ahern, A. T., Williams, L. R., Ehn, M., Mikkilä, J., Canagaratna, M. R., Brune, W. H., Onasch, T. B., Jayne, J. T., Petäjä, T., Kulmala, M., Laaksonen, A., Kolb, C. E., Davidovits, P. and Worsnop, D. R.: Relationship between aerosol oxidation level and hygroscopic properties of laboratory generated secondary organic aerosol (SOA) particles, Geophys. Res. Lett., 37(24), 1–5, doi:10.1029/2010GL045258, 2010.

McFiggans, G., Artaxo, P., Baltensperger, U., Coe, H., Facchini, M. C., Feingold, G., Fuzzi, S., Gysel, M., Laaksonen, A., Lohmann, U., Mentel, T. F., Murphy, D. M., O'Dowd, C. D., Snider, J. R. and Weingartner, E.: The effect of physical and chemical aerosol properties on warm cloud droplet activation, Atmos. Chem. Phys., 6(9), 2593–2649, doi:10.5194/acp-6-2593-2006, 2006.

https://doi.org/10.5194/egusphere-2023-577
Preprint. Discussion started: 7 July 2023

McNeill, V. F.: Aqueous organic chemistry in the atmosphere: Sources and chemical processing of organic aerosols, Environ. Sci. Technol., 49(3), 1237–1244, doi:10.1021/es5043707, 2015.

Mei, F., Setyan, A., Zhang, Q. and Wang, J.: CCN activity of organic aerosols observed downwind of urban emissions during CARES, Atmos. Chem. Phys., 13(24), 12155–12169, doi:10.5194/acp-13-12155-2013, 2013.

Ng, N. L., Herndon, S. C., Trimborn, A., Canagaratna, M. R., Croteau, P. L., Onasch, T. B., Sueper, D., Worsnop, D. R., Zhang, Q., Sun, Y. L. and Jayne, J. T.: An Aerosol Chemical Speciation Monitor (ACSM) for routine monitoring of the composition and mass concentrations of ambient aerosol, Aerosol Sci. Technol., 45(7), 780–794, doi:10.1080/02786826.2011.560211, 2011.

Ogawa, S., Setoguchi, Y., Kawana, K., Nakayama, T., Ikeda, Y., Sawada, Y., Matsumi, Y. and Mochida, M.: Hygroscopicity of aerosol particles and CCN activity of nearly hydrophobic particles in the urban atmosphere over Japan during summer, J. Geophys. Res., 121(12), 7215–7234, doi:10.1002/2015JD024636, 2016.

Petit, J. E., Favez, O., Albinet, A. and Canonaco, F.: A user-friendly tool for comprehensive evaluation of the geographical origins of atmospheric pollution: Wind and trajectory analyses, Environ. Model. Softw., 88, 183–187, doi:10.1016/j.envsoft.2016.11.022, 2017.

Petters, M. D. and Kreidenweis, S. M.: A single parameter representation of hygroscopic growth and cloud condensation nucleus activity, Atmos. Chem. Phys. Atmos. Chem. Phys., 7, 1961–1971, doi:10.5194/acp-7-1961-2007, 2007.

Prakash, J., Lohia, T., Mandariya, A. K., Habib, G., Gupta, T. and Gupta, S. K.: Chemical characterization and quantitativ e assessment of source-specific health risk of trace metals in PM1.0 at a road site of Delhi, India, Environ. Sci. Pollut. Res., 25(9), 8747–8764, doi:10.1007/s11356-017-1174-9, 2018.

Pringle, K. J., Tost, H., Pozzer, A., Pöschl, U. and Lelieveld, J.: Global distribution of the effective aerosol hygroscopicity parameter for CCN activation, Atmos. Chem. Phys., 10(12), 5241–5255, doi:10.5194/acp-10-5241-2010, 2010.

Rai, P., Furger, M., El Haddad, I., Kumar, V., Wang, L., Singh, A., Dixit, K., Bhattu, D., Petit, J.-E., Ganguly, D., Rastogi, N., Baltensperger, U., Tripathi, S. N., Slowik, J. G. and Prévôt, A. S. H.: Real-time measurement and source apportionment of elements in Delhi's atmosphere, Sci. Total Environ., 742, 140332, doi:10.1016/j.scitotenv.2020.140332, 2020.

Randall, D A; Wood, R A; Bony, S; Colman, R; Fichefet, T; Fyfe, J; Kattsov, V; Pitman, A; Shukla, J; Srinivasan, J; Stouffer, R J; Sumi, A; Taylor, K. E.: Climate Models and Their Application, Clim. Chang. 2007 Phys. Sci. Basis. Contrib. Work. Gr. I to Fourth Assess. Rep. Intergov. Panel Clim. Chang. Ed. by S. Solomon al., Cambridge Univ. Press. Cambridge, U. K., New York., Chapter 8(United Kingdom: N. p., p.2007. Web.), 590–662, doi:http://www.ipcc.ch/pdf/assessment-report/ar4/wg1/ar4-wg1-chapter8.pdf, 2007.

Richard, A., Gianini, M. F. D., Mohr, C., Furger, M., Bukowiecki, N. and Minguill, M. C.: and Physics Source apportionment of size and time resolved trace elements and organic aerosols from an urban courtyard site in Switzerland, , 8945–8963, doi:10.5194/acp-11-8945-2011, 2011.

Seinfeld, J. H. and Pandis, S. N.: Atmospheric cemistry and physics: From air pollution to climate change, Second edi., John Wiley & Sons, Inc., 2006.

Shukla, A. K., Lalchandani, V., Bhattu, D., Dave, J. S., Rai, P., Thamban, N. M., Mishra, S., Gaddamidi, S., Tripathi, N., Vats, P., Rastogi, N., Sahu, L., Ganguly, D., Kumar, M., Singh, V., Gargava, P. and Tripathi, S. N.: Real-time quantification and source apportionment of fine particulate matter including organics and elements in Delhi during summertime, Atmos. Environ., 261, 118598, doi:10.1016/J.ATMOSENV.2021.118598, 2021.

Sjogren, S., Gysel, M., Weingartner, E., Baltensperger, U., Cubison, M. J. and Coe, H.: Hygroscopic growth and water uptake kinetics of two-phase aerosol particles consisting of ammonium sulfate , adipic and humic acid mixtures, , 38, 157–171, doi:10.1016/j.jaerosci.2006.11.005, 2007.

Sjogren, S., Gysel, M., Weingartner, E., Alfarra, M. R., Duplissy, J., Cozic, J., Crosier, J. and Coe, and U. B.: Hygroscopicity of the submicrometer aerosol at the high-alpine site Jungfraujoch, 3580m a.s.l., Switzerland, ,

https://doi.org/10.5194/egusphere-2023-577
Preprint. Discussion started: 7 July 2023

7231–7249, doi:10.5194/acp-12-7231-2012, 2012.

Stokes, R. H. and Robinson, R. A.: Interactions in Aqueous Nonelectrolyte Solutions. I. Solute-Solvent Equilibria, J. Phys. Chem., 70(7), 2126–2131, doi:10.1021/j100879a010, 1966.

Su, H., Rose, D., Cheng, Y. F., Gunthe, S. S., Massling, A., Stock, M., Wiedensohler, A., Andreae, M. O. and Pöschl, U.: Hygroscopicity distribution concept for measurement data analysis and modeling of aerosol particle mixing state with regard to hygroscopic growth and CCN activation, Atmos. Chem. Phys, 10, 7489–7503, doi:10.5194/acp-10-7489-2010, 2010.

Sun, Y., Wang, Z., Fu, P., Jiang, Q., Yang, T., Li, J. and Ge, X.: The impact of relative humidity on aerosol composition and evolution processes during wintertime in Beijing , China, Atmos. Environ., 77, 927–934, doi:10.1016/j.atmosenv.2013.06.019, 2013.

Sun, Y., Du, W., Fu, P., Wang, Q., Li, J., Ge, X., Zhang, Q., Zhu, C., Ren, L., Xu, W., Zhao, J., Han, T., Worsnop, D. R. and Wang, Z.: Primary and secondary aerosols in Beijing in winter: Sources, variations and processes, Atmos. Chem. Phys., 16(13), 8309–8329, doi:10.5194/acp-16-8309-2016, 2016.

Swietlicki, E., Hansson, H. C., Hämeri, K., Svenningsson, B., Massling, A., Mcfiggans, G., Mcmurry, P. H., Petäjä, T., Tunved, P., Gysel, M., Topping, D., Weingartner, E., Baltensperger, U., Rissler, J., Wiedensohler, A. and Kulmala, M.: Hygroscopic properties of submicrometer atmospheric aerosol particles measured with H-TDMA instruments in various environments—a review, Tellus B Chem. Phys. Meteorol., 60(3), 432–469, doi:10.1111/j.1600-0889.2008.00350.x, 2008.

Tang, I. N. and Munkelwitz, H. R.: Water activities, densities, and refractive indices of aqueous sulfates and sodium nitrate droplets of atmospheric importance, J. Geophys. Res., 99(D9), 18801, doi:10.1029/94JD01345, 1994.

Tobler, A., Bhattu, D., Canonaco, F., Lalchandani, V., Shukla, A., Thamban, N. M., Mishra, S., Srivastava, A. K., Bisht, D. S., Tiwari, S., Singh, S., Močnik, G., Baltensperger, U., Tripathi, S. N., Slowik, J. G. and Prévôt, A. S. H.: Chemical characterization of PM2.5 and source apportionment of organic aerosol in New Delhi, India, Sci. Total Environ., 745, 140924, doi:10.1016/J.SCITOTENV.2020.140924, 2020.

Topping, D. O. and McFiggans, G.: Tight coupling of particle size, number and composition in atmospheric cloud droplet activation, Atmos. Chem. Phys., 12(7), 3253–3260, doi:10.5194/acp-12-3253-2012, 2012.

Tritscher, T., Jurnyi, Z., Martin, M., Chirico, R., Gysel, M., Heringa, M. F., Decarlo, P. F., Sierau, B., Prévt, A. S. H., Weingartner, E. and Baltensperger, U.: Changes of hygroscopicity and morphology during ageing of diesel soot, Environ. Res. Lett., 6(3), doi:10.1088/1748-9326/6/3/034026, 2011.

Wang, X., Shen, X. J., Sun, J. Y., Zhang, X. Y., Wang, Y. Q., Zhang, Y. M., Wang, P., Xia, C., Qi, X. F. and Zhong, J. T.: Size-resolved hygroscopic behavior of atmospheric aerosols during heavy aerosol pollution episodes in Beijing in December 2016, , 194(September), 188–197, doi:10.1016/j.atmosenv.2018.09.041, 2018a.

Wang, Y., Wu, Z., Ma, N., Wu, Y., Zeng, L., Zhao, C. and Wiedensohler, A.: Statistical analysis and parameterization of the hygroscopic growth of the sub-micrometer urban background aerosol in Beijing, Atmos. Environ., 175(December 2017), 184–191, doi:10.1016/j.atmosenv.2017.12.003, 2018b.

Wester, P., Mishra, A., Mukherji, A., Shrestha, A. B. and Change, C.: The Hindu Kush Himalaya Assessment, edited by P. Wester, A. Mishra, A. Mukherji, and A. B. Shrestha, Springer International Publishing, Cham., 2019.

Wu, Z. J., Poulain, L., Henning, S., Dieckmann, K., Birmili, W., Merkel, M., van Pinxteren, D., Spindler, G., Müller, K., Stratmann, F., Herrmann, H. and Wiedensohler, A.: Relating particle hygroscopicity and CCN activity to chemical composition during the HCCT-2010 field campaign, Atmos. Chem. Phys., 13(16), 7983–7996, doi:10.5194/acp-13-7983-2013, 2013a.

Wu, Z. J., Poulain, L., Henning, S., Dieckmann, K., Birmili, W., Merkel, M., Van Pinxteren, D., Spindler, G., Stratmann, F., Herrmann, H. and Wiedensohler, A.: Sciences ess Atmospheric Chemistry and Physics Climate of the Past Geoscientific Instrumentation Methods and Data Systems Relating particle hygroscopicity and CCN activity to chemical composition during the HCCT-2010 field campaign, Atmos. Chem. Phys, 13, 7983–7996,

https://doi.org/10.5194/egusphere-2023-577
Preprint. Discussion started: 7 July 2023

doi:10.5194/acp-13-7983-2013, 2013b.

Wu, Z. J., Zheng, J., Shang, D. J., Du, Z. F., Wu, Y. S., Zeng, L. M., Wiedensohler, A. and Hu, M.: Particle hygroscopicity and its link to chemical composition in the urban atmosphere of Beijing , China , during summertime, , 1123–1138, doi:10.5194/acp-16-1123-2016, 2016.

Yeung, M. C., Lee, B. P., Li, Y. J. and Chan, C. K.: Simultaneous HTDMA and HR-ToF-AMS measurements at the HKUST supersite in Hong Kong in 2011, J. Geophys. Res., 119(16), 9864–9883, doi:10.1002/2013JD021146, 2014.

Zhang, Q., Jimenez, J. L., Worsnop, D. R. and Canagaratna, M.: A Case Study of Urban Particle Acidity and Its Influence on Secondary Organic Aerosol, Environ. Sci. Technol., 41(9), 3213–3219, doi:10.1021/es061812j, 2007.

Zhang, S. L., Ma, N., Kecorius, S., Wang, P. C., Hu, M., Wang, Z. B., Größ, J., Wu, Z. J. and Wiedensohler, A.: Mixing state of atmospheric particles over the North China Plain, Atmos. Environ., 125, 152–164, doi:10.1016/J.ATMOSENV.2015.10.053, 2016.

Zhang, Y., Tang, L., Yu, H., Wang, Z., Sun, Y., Qin, W., Chen, W., Chen, C., Ding, A., Wu, J., Ge, S. and Chen, C.: Chemical composition , sources and evolution processes of aerosol at an urban site in Yangtze River Delta , China during wintertime, Atmos. Environ., 123, 339–349, doi:10.1016/j.atmosenv.2015.08.017, 2015.

Zhao, P., Du, X., Su, J., Ding, J. and Dong, Q.: Aerosol hygroscopicity based on size-resolved chemical compositions in Beijing, Sci. Total Environ., 716, 137074, doi:10.1016/J.SCITOTENV.2020.137074, 2020.